Positron diffusion in solid and liquid metals

E. Gramsch,* K. G. Lynn,† J. Throwe, and I. Kanazawa‡
Brookhaven National Laboratory, Upton, New York 11973
(Received 2 June 1998; revised manuscript received 17 February 1999)

We made a systematic study of the diffusion of positrons in several liquid and solid metals with a vertical positron beam. Several interesting effects have been observed by studying the line shape parameter *S*, the fraction of positronium formed at the surface, and the diffusion length of positrons in liquids. The *S* parameter and the fraction of positronium created and released at the surface (*F* parameter) were measured as a function of temperature in the solid and liquid phases of Ga, Bi, Na, Sn, In, and Pb. An appreciable change just below or across the melting point in the *S* parameter was measured in metals where positron trapping has not been observed (Ga, Bi, and Sn). In metals where positron trapping occurs in the solid phase, there is a small change or none in the *S* parameter (Pb and In), which indicates that there is only a small change in the nature of the traps. Positron trapping was seen in all the liquid metals, indicating that they have a high density of defectlike sites that trap positrons. The diffusion length of positrons in the liquid was extracted from the experimental data. In Ga, Bi, and Sn, there is a large drop in the diffusion length upon melting; in Pb and In, only a small change or none is seen. In all liquid metals the diffusion length increases as the temperature increases, suggesting that diffusion is related to trapping in temporary fluctuations in the liquid's structure. The positron moves from fluctuation to fluctuation. The size of the traps strongly depends on temperature, and so when it increases, the positron's hopping motion increases. We also measured the reemitted energy spectra of positrons from liquid and solid surfaces. No appreciable change was seen with increasing temperature or when the metals melted. [S0163-1829(99)09521-1]

I. INTRODUCTION

The study of liquid structure and its properties is important for scientific and technological reasons. For instance, many crystals are grown or refined from the molten state, and a better knowledge of the dynamics of impurities can improve crystal quality. However, our knowledge of the liquid structure is much less than our knowledge of the crystalline structure of matter. This is due to the fewer techniques available to study liquids, as well as intrinsic difficulties in formulating models for them.[1–3] Liquid metals can be considered as an ensemble of ions and electrons in a disordered configuration with good electrical and thermal conductivity. In contrast to a solid metal, there is no long- or medium-range order. Short-range order is evidenced by a strong peak in the pair correlation function as determined by x-ray or neutron diffraction experiments.[2] Herein lies the basic difficulty in formulating a model for a liquid: the theory must include the potentials between all pairs of ions. Simplifications that might be included in the model reflecting a periodic arrangement of atoms (as in a crystalline solid) or to a completely disordered structure (as in a gas) are not applicable to a liquid.

It is well known that positrons are strongly sensitive to vacancies and other open-volume defects in solids.[4] Techniques that use positrons as a probe, such as angular correlation or lifetime, have been extensively used to measure formation energies of vacancies and other defects in solid metals.[4–9] Because of the irregular arrangement of ions, a liquid can have regions of low ion density similar to vacancies or voids in a solid. Therefore, positrons can be an ideal probe to study the structure and dynamics of these regions in a liquid.

The sensitivity of positrons to changes caused by melting was demonstrated by early angular correlation[9–11] and lifetime[12,13] studies of liquids. These techniques use high-energy positrons from a radioactive source and probe the bulk region of the liquid. For several metals studied, the lifetime increased 10–40 % on melting. In angular correlation studies,[14] the proportion of conduction-electron annihilations relative to core annihilations was considerably higher in the liquid than in the solid phase. The changes observed upon melting were qualitatively similar to those arising from positron trapping at thermal vacancies in solids.[7] In addition, a large change in annihilation characteristics was observed in metals where vacancy trapping does not occur in the solid phase[12] (for example, gallium and tin), suggesting that the disorder creates regions of low ion density, similar to vacancies in solids, that can trap positrons. Metals that show large changes in angular correlation and lifetime in the solid phase upon heating (for example, lead or indium) demonstrate a small or no change upon melting.[15]

In contrast to these techniques, which utilize positrons with a wide energy distribution ($\delta E > 100$ keV), positron beams have narrow energy ($E < 10$ eV) distribution and small size (a few millimeters).[6] Furthermore, positrons can be implanted into the sample at a depth that is known and, most important, can be controlled. Preliminary studies of liquid metals using low-energy positrons have shown several interesting results,[16] indicating that this technique is very powerful to study the structure of liquids.

Upon melting, the metal loses its crystalline structure, becoming a disordered array of atoms. There is an increase in the number of traps (considered as regions of low ion density), and positron localization increases. Because the fraction of trapped positrons probably increases as the sample

melts, the mean free path will be shorter than in the solid phase and the diffusion coefficient will decrease. The diffusion of thermalized positrons in solids is determined by their interactions with phonons,[6,17–21] impurities, or by trapping (in vacancies, voids, or other defects). In a defect-free metal, the diffusion coefficient D_+ for positrons has a temperature dependence[17] of $D_+ \sim T^{-1/2}$. In some metals, at temperatures close to the melting point, positrons become trapped at thermally generated vacancies, and the effective diffusion coefficient decreases even faster.

In contrast, in the liquids we studied, the diffusion coefficient increases with temperature. This surprising result suggests that a different mechanism is involved in the interactions of positrons with the liquid. Kanazawa[22] recently proposed a qualitative explanation for the increase with temperature of the positron diffusion length in liquid metals. In this model, as the temperature increases, the effective mass of the positron decreases due to the restoration of the spontaneously broken density around the positron. Seeger[23] suggested that the interaction of the positron with a liquid is via two polaronic states, with large effective masses that depend on the material. Upon heating, positrons that are in the high-m^+ polaron state (as in Ga) increase their hopping motion, therefore increasing the diffusion length. Positrons that are in the low-m^+ polaron state (as in Bi) have a diffusion length with a weaker temperature dependence.

To better understand the mechanism of diffusion in liquids, we systematically studied the diffusion characteristics of positrons in several liquid and solid metals. A vertical positron beam was designed and built to study low-melting-temperature metals under ultrahigh-vacuum conditions. Of considerable interest to us was the study of surface defects (or regions of low ion density), positron and positronium states at the surface, and the relation between the diffusion coefficient and density fluctuations in liquids.

In Sec. II, we briefly discuss the different interactions of positrons with solid and liquid metals. The observable parameters are defined in this section. We assume that the motion of the thermalized positron is a random walk and describe its motion with the diffusion equation. The fitting routine used to obtain the diffusion length of positrons in liquid metals is described.

In Sec. III, we describe the vertical positron beam and the unique characteristics that allow it to measure liquids.

In Sec. IV, we present the experimental results. The metals are separated into two groups according to whether or not the onset of trapping has been observed in the solid phase. The first group comprises Ga, Bi, Na, and Sn in which positrons do not become trapped in thermally generated vacancies in the solid phase, but are trapped in the liquid phase. Consequently, there are large changes in the S and F parameters and in the diffusion coefficient. The second group is formed by Pb and In, in which positrons become trapped at thermally generated vacancies in the solid phase, and there are no changes upon melting.

In Sec. IV A, the experimental values for the line shape parameter S and positronium fraction F versus energy are presented. Using these measurements, we can determine the state of the positron in the solid or liquid phase (freely diffusing or trapped). We discuss the sensitivity of positrons to the melting transition and the formation of positronium at the surface of the liquid. The S and F parameters are measured as a function of temperature for several incident energies, and the results are compared to previous studies of positron lifetimes and Doppler broadening in liquids. A surface state is shown to exist in some liquids, and positronium formation is observed at several surfaces.

In Sec. IV B, we present results of diffusion length measurements in solid and liquid metals. The increase in the diffusion length with temperature is discussed in terms of positron hopping between traps and is related to density fluctuations in the metal or to thermal desorption of the positrons from the traps. However, to obtain more quantitative information of the fluctuations in liquid metals, we still need a theoretical model relating the diffusion length to density fluctuations.

We discuss our measurements of nonthermal positron reemission from the surface of liquid and solid metals in Sec. IV C. At $\approx$50 eV, a small fraction (5–15 %) is reemitted from Bi, Sn, and In. This fraction is unchanged upon melting.

The conclusions and suggestions for future studies are given in Sec. V.

II. DIFFUSION MODEL

A. Diffusion of thermal positrons

When monoenergetic positrons from a beam reach thermal energies $E_{\rm th}=\frac{3}{2}k_BT$, their spatial distribution within the sample in the incident direction (z) can described by a Makhovian distribution[24]

$$P(z)=\frac{mz^{m-1}}{z_0^m}\exp[-(z/z_0)^m], \tag{1}$$

where $z_0=\overline{z}/\Gamma(1/m+1)$; Γ is the gamma function. The distribution is isotropic in a plane parallel to the surface. The mean implantation depth $\overline{z}$ is assumed to be a power law:

$$\overline{z}=AE^n, \tag{2}$$

where E is the incident energy of the beam and A is a constant, discussed below. The relation (2) between incident energy and mean implantation depth gives us a depth-sensitive *probe*, which is essential for defect profiling, study of surface states, or surface melting. The value of n depends on the energy and varies from 1.16 at 3 MeV to 1.68 at 10 keV.[25,26] From Monte Carlo simulations[21] and from studies of multilayer structures,[26,27] it was found that $n\approx 1.6$ for positrons, but there are indications that this value depends on the material.[28]

The shaping parameter m is close to 2 as shown from fits to Monte Carlo simulations[21] and from studies of multilayer structures.[26] Following Ref. 6, in this paper we use $A=4.0/\rho\,[\mu\text{g/cm}^2]$.

B. Nonthermal positrons

Before complete thermalization, a small fraction of positrons can return to the surface or become trapped at defects in the bulk of the sample. In lifetime measurements,[29,30] nonthermal trapping of positrons was proposed to explain a drop with temperature in λ_f, the annihilation rate of untrapped

positrons. Nonthermal positron trapping in vacancies was observed only recently[25,31] and was shown to affect the analysis of the diffusion length of positrons. These experiments also showed that trapping is very efficient and can occur faster than 10^{-15} s. A recent theoretical model[32] showed resonances in the trapping rate at energies of about 1–2 eV that can only enhance nonthermal trapping. The analysis of lifetime data,[33] as well as calculations of diffusion length, is affected by the fraction of nonthermal positrons.

Nonthermal positron and positronium emission are not included in the diffusion model. The effect of nonthermal reemission of positrons in analyzing the diffusion length is discussed in Sec. IV B.

C. Diffusion model

When positrons have thermal energies, scattering with phonons is isotropic, with typical mean free paths of about 100 Å. Since the mean free path[34] for positron scattering is smaller than typical implantation depths (about 1000 Å), it is generally assumed that the motion of the positron is adequately described by the diffusion equation.

Mathematically, this model of positron motion can be represented by the diffusion equation in one dimension:[35,36]

$$\frac{\partial N_p(z,t)}{\partial t} = D_+ \frac{\partial^2 N_p(z,t)}{\partial z^2} - \lambda_{\text{eff}} N_p(z,t), \tag{3}$$

where z is the distance from the surface, N_p is the positron density, D_+ is the positron diffusion coefficient, $\lambda_{\text{eff}} = \lambda_b + \lambda_t$ is the effective annihilation rate of the positron, λ_b is the bulk annihilation rate, and λ_t is the trapping rate. The formula does not include thermal detrapping of the positron, which, in most solids, is small. We discuss the relevance of detrapping in liquids in Sec. IV B.

By solving Eq. (3), we can obtain the fraction F_s of positrons that return to the surface for a given incident energy. The connection between theory and experiment is given by F_s, and this value can be directly compared with the experimental results.

At the surface, the interaction of positrons with ions, surface, and core electrons produce a potential well that traps the positrons.[37] Trapped positrons eventually annihilate with a surface electron or form positronium an leave the surface.

During diffusion, some positrons approach the surface before annihilation, where several interactions can occur:[6] (1) Binding to the surface potential well. (2) Free reemission if the positron's energy is higher than its work function ϕ_+ or if ϕ_+ is negative (W, Ni, Cu). This effect is more pronounced at low energies ($E_{\text{inc}} < 4$ keV). The signal from these positrons can affect the analysis of the results and is discussed in Sec. IV B. (3) Positronium emission. If the sum of the electron and positron work functions is less than the binding energy of Ps (6.8 eV), positrons can pick up a surface electron and be reemitted as Ps or as excited states of Ps (Ps^*, Ps^-). Nonthermal positrons also can pick up an electron and be reemitted with higher energies. (5) Internal reflection at the surface. The alkali metals have a low electron density, perhaps reducing the extent to which the electrons penetrate out into the vacuum. This, in turn, tends to create a potential well outside the surface that is too narrow to have bound states.[38] Therefore, a positron reaching the surface will be reflected back to the bulk.

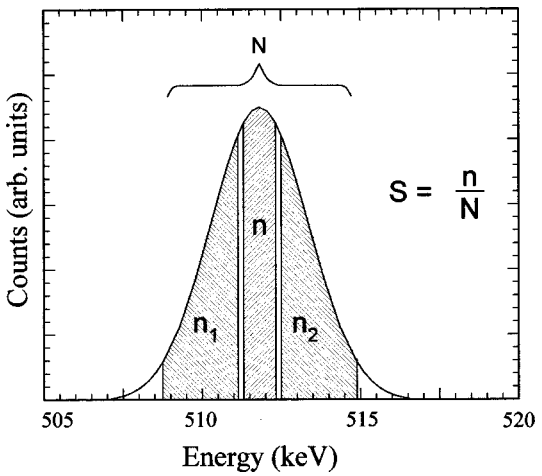

FIG. 1. Illustration of the areas used to define the S (line shape) parameter. $S = n/N$.

D. Observables

The technique used in this study consists of measuring the energy resolution of the annihilation the γ rays. The spectrum obtained is a convolution of the energy resolution of the detection system and the Doppler broadening of the annihilating γ rays (Fig. 1).

Because of the momentum of the electron at the site of annihilation, the annihilation radiation exhibits a Doppler shift around the mean energy value (511 keV). In a metal, typical valence-electron energies are of the order of the Fermi energy (3–10 eV), core-electron energies are much higher, while a thermalized positron has only a few meV ($\sim$0.04 eV). A localized positron has higher energy than a thermalized positron, but still much smaller than an electron. Therefore, the γ rays resulting from the annihilation will have a spread in energy and angle that is proportional to the momentum of the electron only.

When positrons annihilate with core electrons, the Doppler broadening is large because of the relatively large momentum of the core electrons, and the peak is broader. When the positron annihilates with a low-momentum electron (conduction electron), the peak is narrow. These two effects are characterized by the line shape parameter S, introduced by MacKenzie *et al.*[39] and defined as the area of a central segment of the 511-keV peak divided by the total area (Fig. 1).

If there are various annihilation modes (in defects, bulk, surface, or from Ps), each with a probability F_i, having a line shape S_i, the observed S is

$$S = \frac{\Sigma S_i F_i}{\Sigma F_i}. \tag{4}$$

The superposition property of the S parameter,[39] Eq. (4) is essential for studying the diffusion length of positrons because the probability F_s of positrons reaching the surface can be obtained by solving the diffusion equation. The probability of positrons annihilating in the bulk is just $1 - F_s$, and the result from an experiment will be

$$S=\frac{S_sF_s+S_M(1-F_s)}{\Omega}, \tag{5}$$

where Ω is a normalization factor defined below, S_s is the S parameter from positrons annihilating at the surface, and S_M is associated with positrons annihilating in the bulk. The second term, in general, has contributions from positrons annihilating in the defect-free bulk (S_{bulk}) and trapped at defects (vacancies, voids, etc.). If F_{bulk} and F_t are the free and trapped fractions, the bulk S is given by $S_M=S_tF_t+S_{\text{bulk}}F_{\text{bulk}}$.

The surface term S_s has several contributions. Positrons can annihilate while trapped at the surface state, after forming Ps, or after being emitted as free positrons. Two types of Ps atoms can be formed, each with a different decay scheme. Twenty-five percent are para-Ps, the singlet spin state, which has a short lifetime ($\sim$125 ps) and decays via two γ rays; thus, its signal falls into the 511-keV annihilation peak. Seventy-five percent of the Ps are ortho-Ps, the triplet spin state that has a long lifetime (142 ns), and decays predominantly via three γ rays; thus, the signal has a distribution in energy below 511 keV. Ortho-Ps atoms exist long enough to travel far from the surface, and a small fraction is not detected. Only para-Ps atoms contribute to the S parameter. Therefore, an expression for S at the surface is given by

$$S_s=\frac{1}{4}F_0S_{\text{Ps}}+(1-F_0)S_{ss}, \tag{6}$$

where F_0 is the fraction of positrons arriving at the surface that form Ps. S_{Ps} corresponds to the S parameter associated with the fraction $\frac{1}{4}F_0$ of positrons that annihilate after forming para-Ps (the fraction $\frac{3}{4}F_0$ that forms ortho-Ps does not contribute to S_s because the energy of each emitted γ ray is less than 511 keV). S_{ss} is associated with the fraction $(1-F_0)$ annihilating with valence electrons from the surface state. Because of the low center-of-mass momentum of the Ps atom, S_{Ps} is higher than S_{ss}.

In all metals that we studied, only a small fraction of positrons escape from the sample before complete thermalization (less than 14% at energies below 600 eV). Thus the S parameter arising from nonthermal positrons that escape and eventually return to the sample can be neglected. The measured nonthermal fraction is discussed in Sec. IV C.

The calibration factor Ω is the sum of the different annihilation modes that contribute to S:

$$\Omega=(1-F_s)+F_s\left(1-\frac{3}{4}F_0\right). \tag{7}$$

The positronium fraction, i.e., the fraction of positrons that forms positronium for a given incident energy and temperature, is $F(E,T)=F_s(E,T)F_0$. Because of the factor Ω in the definition of S, the positronium fraction is a nonlinear function of S.

The positronium fraction can also be determined experimentally:[40]

$$F=\left(1+\frac{P_1}{P_0}\frac{(R_F-R_0)}{(R_1-R_F)}\right)^{-1}, \tag{8}$$

where $R_F=(T_F-P_F)/T_F$, $R_0=(T_0-P_0)/T_0$, and $R_1=(T_1-P_1)/T_1$, which are independent of the beam's intensity. T is the total number of counts of the spectrum below 511 keV, and P includes only the counts under the photopeak. T_1 is the total number of counts when $F=1$, and T_0 the counts when $F=0$. P_1 and P_0 are defined accordingly.

R_0 is calculated from the total energy spectrum and P_0 from the 511-keV peak at high incident energies (when no positrons can return to the surface). P_1 and R_1 are more difficult to determine because their values have to be extrapolated to zero incident energy, under very clean surface conditions, at high temperature, and when all positrons are thermally desorbed as Ps. Even then it is difficult to determine R_1 and P_1 with confidence.[40]

E. Fitting procedure

Equation (5) can be fitted to the S parameter data to obtain the diffusion length $L_+=\sqrt{D_+\tau_{\text{eff}}}$ of positrons at a given temperature. The fitting routine used in this work was developed by van Veen *et al.*[41] and is a fast numerical scheme designed to solve the diffusion equation (3). This scheme allows several parameters related to the implantation profile to be fitted: m, n, and A parameters, mean depth, trapping rates, and electric fields in layered materials. The positron diffusion parameters also are fitted: S_{bulk}, S_s, and the diffusion length L_+. The last parameter is defined in terms of the effective lifetime and the diffusion coefficient, $L_+=\sqrt{D_+\tau_{\text{eff}}}$. More detailed information is given by van Veen *et al.*[41]

III. EXPERIMENT

The experiments were performed with a magnetically guided vertical positron beam designed to study the interaction of positrons with low-vapor-pressure liquids at ultrahigh vacuum.[42,75] High-energy positrons are obtained from a radioactive source and are moderated to a few eV. Subsequently, they are guided to the sample and implanted at the desired energy. The resolution of the beam is 1 eV at 200 eV. The transport system, consisting of nine coils that magnetically guide the positrons to the target, is mounted vertically to allow study of liquid samples. The source and $\mathbf{E}\times\mathbf{B}$ chamber can be floated up to 25 kV, while the sample is kept at ground or near ground potential.

The sample is located in the lower chamber, mounted in a 24-in. manipulator. The sample is heated with a noninductively wound W wire electrically isolated from the sample holder. The maximum temperature to which the sample can be heated is $\sim$600 °C. The temperature is measured with a type-K thermocouple attached to the sample holder. Temperature fluctuations depend on the sample's temperature. Above 150 °C, fluctuations from the set point are less than 1°. At room temperature, the fluctuations are 2–5 °C. For cooling, there is a liquid nitrogen line that fills a small Dewar close to the sample. The lowest temperature attainable is ~-100 °C.

A high-purity intrinsic Ge detector located outside the chamber, on one side of the sample, is used for measuring Doppler broadening and the positronium fraction. The resolution obtained with this detector is 1.4 keV full width at half

TABLE I. Lattice structure and other physical characteristics of the metals studied. orc=orthorhombic, rhl=rhombohedral, bcc=body-centered cubic, fct=tetragonal, and fcc=face-centered cubic. Z is the number of valence electrons; T_m is the melting temperature. Trapping refers to trapping in thermally generated vacancies in the solid phase.

Metal	Lattice	Z	T_m (°C)	Trapping in vacancies
Ga	orc	3	29.8	no
Bi	rhl	5	273.3	no
Na	bcc	1	95.7	no
Sn	fct	4	232.0	no
Pb	fcc	4	327.5	yes
In	fct	3	156.6	yes

maximum (FWHM) at 477 keV (^{7}Be source).

A p-i-n photodiode coupled to a CsI(Tl) scintillator is located below the sample and monitors the stability of the beam. When the beam does not hit the sample, more positrons annihilate in the bottom of the chamber, increasing the count rate in this detector.

Liquid samples present geometric constraints; the sample's surface must be horizontal. Therefore, the surface analysis equipment must be usable without rotating the sample; this configuration is achieved by mounting the Auger analyzer and low-energy electron diffraction (LEED) system vertically. An ion gun is located in the same chamber and allows cleaning the sample *in situ*.

The beam transport is achieved with a magnetic field of ~100 G produced by nine solenoid magnets. A gradient in the field is established to focus the beam and reduces its cross sectional area at the sample.

The current in the two solenoids positioned above the sample is controlled by computer. When the incident energy of the beam is changed, the area of the spot and its position changes slightly. To correct this effect, the magnetic field produced by two magnets above the sample is adjusted for each incident energy. The effective diameter of the beam at the sample is ~3 mm. The beam moves sideways less than 2 mm when the energy varies from 100 eV to 25 keV.

IV. RESULTS

A. Temperature dependence of S and F

We studied several liquid metals to identify the variables that contribute to the diffusive motion of positrons. As with solids, we expected that positrons will diffuse freely or be trapped at defects or at the surface of the liquid.

The metals studied can be classified according to the state of the positron in the solid phase. The first group of metals, Ga, Bi, Na, and Sn, is composed of those in which thermal vacancy trapping has not been observed in the solid phase, either by lifetime studies[12,42,43] or by angular correlation studies.[9,15,44] The second group, Pb and In, is composed of those where positron trapping is observed at thermally generated vacancies.[15] Table I shows some of the relevant properties of these metals.

In the liquid phase, most likely there are regions of low ion density with varying sizes. Therefore, trapping is likely to occur in all metals. For untrapped positrons, diffusive motion could be related to lattice scattering, as in the solid phase.

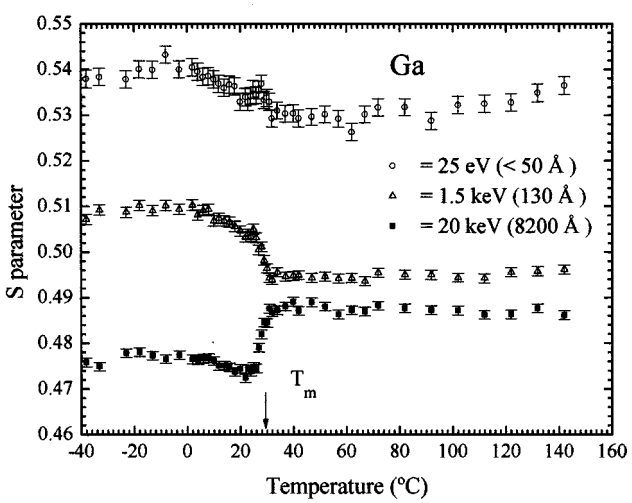

FIG. 2. S parameter in Ga for three incident energies as function of temperature. $E=25$ eV corresponds to positrons implanted close to the surface ($\overline{z}<50$ Å), $E=20$ keV are positrons implanted in the bulk ($\overline{z}\approx 8200$ Å), and $E=1.5$ keV positrons implanted at $\overline{z}\approx 130$ Å; this curve has contributions from positrons annihilating in the bulk and surface.

1. Measurements of S and F as a function of temperature for Ga, Bi, Na, and Sn

a. Gallium. Solid and liquid gallium has been studied using positron lifetime[12] and angular correlation[44] techniques. Previous measurements of the F parameter in liquid and solid Ga using a positron beam did not show a significant difference between these phases.[45] However, our preliminary study of solid and liquid Ga shows a large difference in the S parameter.[16]

Gallium is an interesting metal because it has a low melting point, 29.8 °C, and it contracts 3.1% on melting; its vapor pressure at 500 °C is only 2×10^{-9} torr. These characteristics allow studies over a large range of temperature in the liquid phase at ultrahigh vacuum ($<10^{-9}$ torr). The Ga sample was obtained from ROC/RIC, Ca, 99.999% purity. Before placing it in vacuum, it was etched in 50% nitric acid, 50% distilled water,[46] until its surface became shiny. Then it was cooled under vacuum to -10 °C, sputtered with argon at a pressure of 4×10^{-4} torr for 1 h, and annealed at 500 °C for 12 h. No trace of contaminants was detected with retarding field Auger-electron spectroscopy. This cleaning procedure was performed on all samples before any of the measurements; the Auger spectra did not show contaminants for any of the samples. The spectra are not shown here to save space.

The S parameter was measured as function of the temperature at three incident energies (Fig. 2). The three curves correspond to positrons implanted close to the surface $\overline{z}<50$ Å ($E=25$ eV), in the bulk $\overline{z}\approx 8200$ Å ($E=20$ keV), and at an intermediate point where there are contributions from the surface and the bulk, $\overline{z}\approx 130$ Å ($E=1.5$ keV). The mean implantation depth was calculated from the incident energy using Eq. (2).

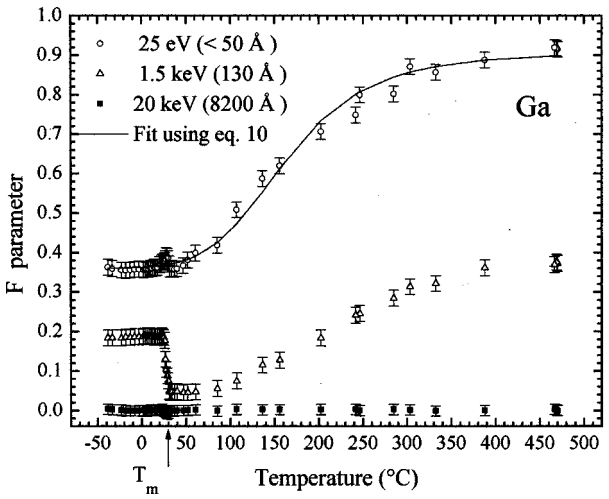

FIG. 3. Positronium fraction (F) in Ga as function of temperature. The first curve is for $\overline{z}<50$ Å, the second curve is for $\overline{z}\approx 130$ Å, and the lower curve is for $\overline{z}\approx 8200$ Å. The solid line is a nonlinear fit using Eq. (10).

The S parameter at the surface ($E=25$ eV) does not significantly change at the melting temperature, suggesting that the ratio of positrons forming Ps or annihilating at the surface is not altered; i.e., it is independent of the crystalline structure. The small fluctuation observed at the melting point could be associated with changes in the geometry of the sample or by partial melting due to variations in temperature across the material; also, solid and liquid phases in Ga can coexist at temperatures close to the melting point. Interestingly, the density of electron states increases significantly[47] near the Fermi energy when Ga melts, suggesting that there are more energetic electrons available to pick up the positrons and form positronium; an increase in positronium formation was expected on melting, but this was not observed.

The positronium fraction curves are shown in Fig. 3 for the same incident energies. The first curve ($E=25$ eV) shows that positronium begins to be thermally desorbed at ≈ 50 °C. Thermal desorption of Ps in liquids has not been observed previously. These data show that a positron surface state can exist on disordered surfaces. The small change in positronium fraction at the melting point could reflect local melting or impurities being released from the surface.

We turn now to a quantitative treatment of positronium desorption. The activation energy of positronium, E_a, is related to the binding energy of positrons to the surface trap, E_b, the energy necessary to extract an electron from the surface, ϕ_-, and the energy released (6.8 eV) when Ps is created in a vacuum:[48]

$$E_a=\phi_-+E_b-6.8 \text{ eV}. \tag{9}$$

Typical values of E_b are 2–3 eV. The activation energy for desorption of positronium, E_a, can be calculated by fitting the temperature dependence of the fraction of positrons arriving at the surface that form Ps:[49]

$$F(E,T)=F_e+\frac{\Gamma \exp(-E_a/k_BT)}{\lambda+\Gamma \exp(-E_a/k_BT)} f_{ts}, \tag{10}$$

where F_e is a fraction of the nonthermal positrons that reach the surface and are emitted as Ps directly (nonthermal Ps). The second term in Eq. (10) is the fraction of positronium emitted from the surface state, with f_{ts} being the fraction of positrons trapped at the surface. It is generally assumed that the desorption rate[49,50] is $\Gamma \exp(-E_a/k_BT)$, where λ is the annihilation rate of positrons trapped at the surface state. The model has been fitted to the experimental values of the Ps fraction in Fig. 3 with a nonlinear fitting routine, using F_e, f_{ts}, E_a, and Γ/λ as free parameters. The solid line in Fig. 3 shows the fitted results, which are $E_a=0.35(0.03)$ eV, $F_e=0.36(0.01)$, $f_{ts}=0.55(0.01)$, and $\Gamma/\lambda=1.0(0.4)\times 10^4$. These results are also shown in Table III.

The electron work function in metals depends on the crystallographic direction of the surface; the difference between different orientations is about 5%. However, the values of the work function obtained by different experimental methods[51] also differ by 5%. Therefore, we used the average from different orientations. From Ashcroft and Mermin,[51] the electron work function in Ga is $\phi_-=3.96$ eV. From Eq. (10), we obtain for the positron binding energy $E_b=3.19(0.03)$ eV. This value is higher than the theoretical value $E_b=2.3$ eV, obtained by Nieminen and Hodges.[52] However, these authors used an averaged electron density to determine the correlation energy E_{corr}, and it was shown later[53] that this method gives variations in the absolute values of the positron work function of up to 1 eV.

The curve at $E=1.5$ keV in Fig. 2 shows the S parameter for positrons implanted at $\overline{z}\approx 130$ Å. This curve has contributions from positrons that annihilate in the surface and in the bulk. In Ga, the fraction of trapped and free positrons increases upon melting and the S parameter drops because fewer positrons can reach the surface, indicating that the diffusion length reaches a minimum.

The bulk value of S for Ga in Fig. 2 ($E_{\text{inc}}=20$ keV) increases at the melting point due to positron trapping.[12,44] An increase[12] in the bulk lifetime of Ga, from 190 to 260 ps, also suggests that positrons become trapped in liquid Ga. We note that these traps do not affect positrons annihilating at the surface; because no change is seen in S_s.

In solid Ga, positrons do not get trapped in thermal vacancies[44] possibly because Ga has a very open-packed structure; orthorhombic Ga has a coordination number[47] $N_c=7$. Therefore, because of the large separation between atoms, potential wells capable of trapping positrons either are not created[54] or they are too shallow. On melting, Ga contracts by 3.1%, and the coordination number increases to $N_c=9-10$.[47] Despite this decrease in the average interatomic spacing, previous studies showed that trapping does occur in the melt.[12]

Kishimoto and Tanigawa's[55] two-parameter correlation of the lifetime of positrons and energy of the annihilation radiation suggests that more than one annihilation mode coexists in the melt. One mode is short lived, with a narrow momentum distribution, which is attributed to trapping and annihilation in solidlike clusters in the liquid; the other is long lived, with a broad momentum distribution,[55] attributed to trapping in vacancylike defects. These two modes of annihilation also were evident from the small decrease in the lifetime of positrons in liquid Ga as the temperature increased.[12] Our results show only a small decrease in S_M as temperature

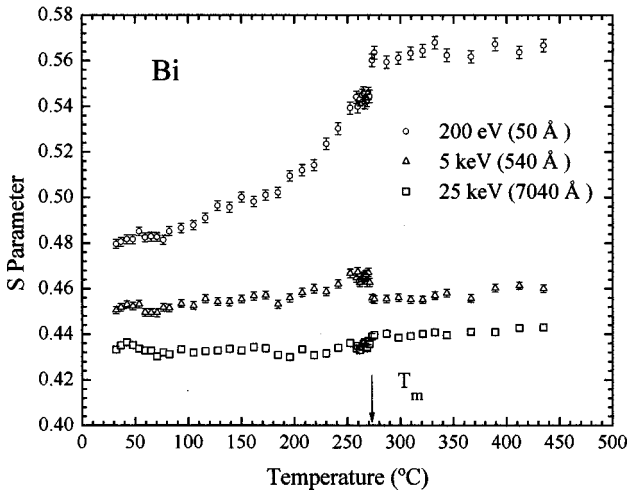

FIG. 4. *S* parameter for Bi plotted as function of temperature for three incident energies. $E=200\,\mathrm{eV}$ corresponds to positrons implanted at $\bar{z}<50\,\text{Å}$, $E=5\,\mathrm{keV}$ to positrons implanted at $\bar{z}\approx 540\,\text{Å}$, and $E=25\,\mathrm{keV}$ corresponds to $\bar{z}\approx 7040\,\text{Å}$.

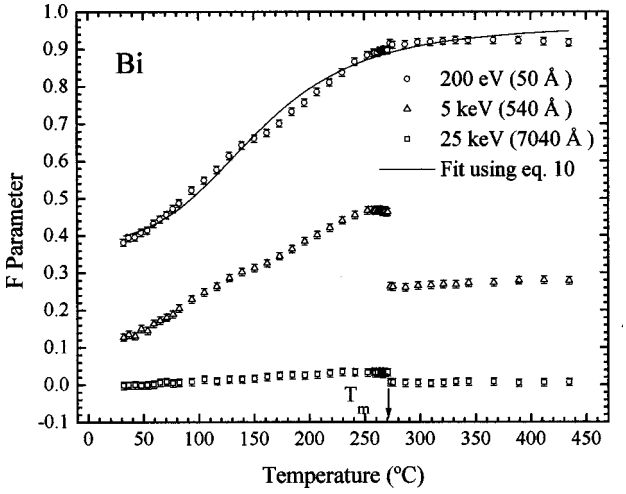

FIG. 5. Positronium fraction in Bi as a function of temperature at the same incident energies as in Fig. 5. The solid line is a nonlinear fit using Eq. (10).

increased; so we cannot conclude that there are two modes of annihilation. Rather, they could reflect an increase in the average size of the traps.

b. Bismuth. Bi is a semimetal with low melting point $T_m=273.3\,^{\circ}\mathrm{C}$, which also contracts on melting (3.3%). Its vapor pressure just above the melting point is $\approx 1\times 10^{-10}\,\mathrm{torr}$; its density at room temperature is 9.8 $\mathrm{g/cm^3}$. The Bi sample was obtained from Aesar/Johnson Matthey, 99.9999% purity. Before placing it in the vacuum, it was cleaned with a procedure similar to Ga.

As in Ga, previous studies with Bi (Ref. 56) showed that there was no trapping of positrons in thermally generated vacancies in the solid phase. Therefore, in solid Bi, the bulk *S* parameter increases slightly following the thermal expansion of the lattice.[56]

The *S* parameter (Fig. 4) at low incident energy $E=200\,\mathrm{eV}$ corresponds to positrons implanted close to the surface ($\bar{z}<50\,\text{Å}$). This curve starts to increase at $\sim 80\,^{\circ}\mathrm{C}$ and levels off above the melting point. At the melting point there is a jump which is due to a small increase in positronium fraction. This increase is seen in Fig. 5.

The curve at $E=5\,\mathrm{keV}$ in Fig. 4 shows the *S* parameter from positrons implanted at $\bar{z}\approx 540\,\text{Å}$ and has a similar behavior as for Ga. At the melting point, the *S* parameter drops because fewer positrons can return to the surface, indicating that the diffusion length decreases on melting.

The positronium fraction is shown in Fig. 5 for the same incident energies as Fig. 4. The formation of thermally activated Ps is clearly seen in the curve at $E=200\,\mathrm{eV}$. Using Eq. (10), the curve at $E=200\,\mathrm{eV}$ in Fig. 5 can be fitted to obtain the formation energy of positronium. The results obtained are $E_a=0.32(0.03)\,\mathrm{eV}$, $F_e=0.38(0.01)$, $f_{ts}=0.58(0.02)$, and $\Gamma/\lambda=6(1)\times 10^3$. The solid line shows the fitted results (see also Table III). The electron work function[51] of Bi is $\phi_-=5.4\,\mathrm{eV}$. Using Eq. (9), we can obtain the binding energy of positrons to the surface trap, which is $E_b=2.72(0.01)\,\mathrm{eV}$.

The change in positronium fraction at the melting point seen in the third curve of Fig. 5 ($E=25\,\mathrm{keV}$) reflects $\sim 3\%$ of the positrons reaching and annihilating at the surface of the solid. Upon melting, all positrons annihilate in the bulk of the sample.

The curve at $E=25\,\mathrm{keV}$ in Fig. 4 ($\bar{z}\approx 7040\,\text{Å}$) shows a slow increase with temperature and a small jump upon melting. There are two competing effects in this jump. One of them is the decrease in the positronium fraction in the liquid (it can be seen in Fig. 6), which tends to reduce the *S* parameter. The other effect is probably an increase in vacancy trapping[57] or a change in the electronic configuration[58] which tends to increase the *S* parameter. The last effect is dominant because the total change is positive.

c. Sodium. Na is an alkali metal with a low melting point $95.7\,^{\circ}\mathrm{C}$; its vapor pressure at $130\,^{\circ}\mathrm{C}$ is $\approx 4\times 10^{-8}\,\mathrm{torr}$. The vapor pressure increases very rapidly as temperature increases. Therefore, we could only obtain measurements below $250\,^{\circ}\mathrm{C}$. Sodium reacts easily with oxygen and hydrogen, and is very hard to keep clean, even at a pressure of

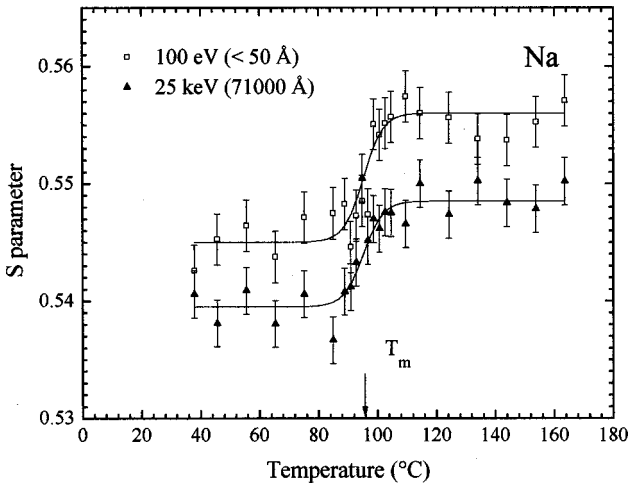

FIG. 6. *S* parameter in Na for positrons implanted close to the surface ($E=100\,\mathrm{eV}$) and deep in the bulk ($E=25\,\mathrm{keV}$) as a function of temperature. Both curves show similar features and are close to each other, indicating that positrons annihilate in the bulk in both cases. The solid line is a guide to the eye.

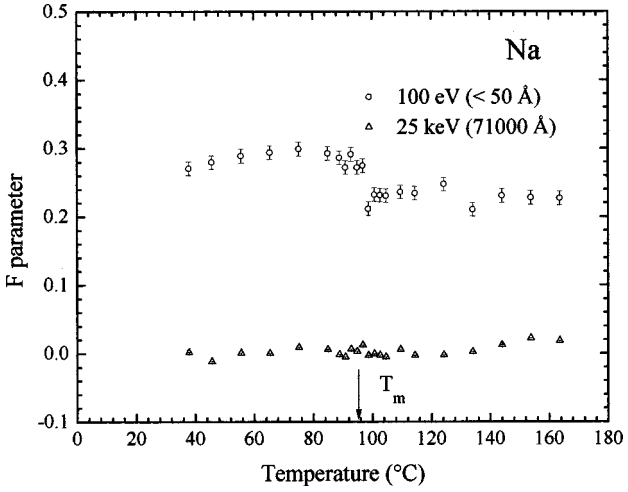

FIG. 7. Positronium fraction in Na as a function of temperature for the same incident energies as in Fig. 6.

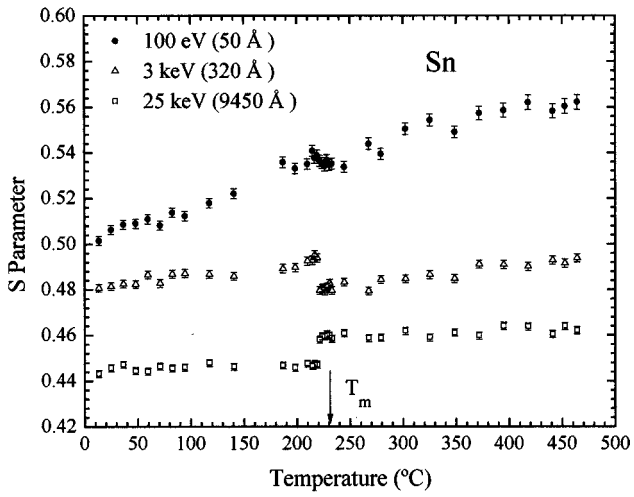

FIG. 8. *S* parameter for solid and liquid Sn as function of temperature at three incident energies. $E=100$ eV corresponds to positrons implanted at $\overline{z}<50$ Å, $E=3$ keV corresponds to $\overline{z}\approx 320$ Å, and $E=25$ keV corresponds to $\overline{z}\approx 9450$ Å.

2×10^{-9} torr, our normal running conditions. Therefore, to ensure a clean sample, a sealed ampule from Aesar/Johnson Mathey, 99.95% purity, was inserted into the vacuum system. When the pressure reached $\approx 1\times10^{-9}$ torr, the tip of the ampule was broken and heated until liquid Na poured into the sample holder; a large, clean meniscus was obtained. The surface subsequently was cleaned of impurities by skimming it with a flat, stainless-steel blade. Auger spectra taken before and after measurements showed that the surface of the sample remained clean.

Previous theoretical studies[34,53] predicted a large positive value for the positron work function, $\phi_+=5.6$ eV for sodium, and a positive value for the positronium work function, $\phi_{Ps}\approx 0.4$ eV. Therefore, no positron or positronium emission from the surface was expected. In addition, it was calculated that there would be no bound states at the surface because the potential is too narrow.[34] In consequence, all thermal positrons reaching the surface from the inside of the metal would be reflected back and eventually annihilate in the bulk. This effect can be seen in Fig. 6, where we show the *S* parameter for two incident energies. The figure shows a very small difference between positrons implanted close to surface ($E=100$ eV, $\overline{z}<50$ Å) and positrons implanted deep into the bulk ($E=25$ keV, $\overline{z}=71\,000$ Å) because most annihilate in the bulk. The solid line in Fig. 6 is a guide to the eye.

The higher value of the *S* parameter for $E=100$ eV than for $E=25$ keV is associated with nonthermal positronium formation. Figure 7 also shows a small fraction of (nonthermal) positronium ($\sim$20%) in the solid and liquid phases.

The increase at the melting point of the *S* parameter for both curves is associated with positron trapping in liquid Na (same as Ga and Bi). As mentioned before, trapping in solid Na has not been observed: trapping in liquid Na was observed with lifetime techniques.[12] In those experiments the lifetime increased from $\approx$263 to $\approx$278 ps upon melting.

The measured *S* parameter is thus given by $S=S_M$, which is independent of the incident energy. In consequence, it is not possible to extract the diffusion length from the experimental data.

In Fig. 7, the Ps fraction is plotted as a function of temperature. At low incident energies, a small fraction is desorbed from the surface, which, we believe, is due to nonthermal positrons. The decrease upon melting may be due to a decrease in the density of electron states at the Fermi energy, which reduces the probability of picking an electron to form Ps.

d. Tin. Sn is a metal with a low melting point 232.0 °C. Its density is $\rho=7.3$ g/cm^3, and its vapor pressure at $T=900$ °C is $\sim 1\times10^{-6}$ torr. Previous studies[14,59] showed no vacancy trapping in the solid phase, even at temperatures close to the melting point.

The *S* parameter, measured as a function of temperature for three incident energies, is shown in Fig. 8. As with Ga and Bi, we can calculate an approximate implantation depth using Eq. (2). The curve at $E=100$ eV corresponds to positrons implanted less than 50 Å from the surface. $E=3$ keV corresponds to positrons implanted at $\overline{z}\approx 320$ Å and $E=25$ keV to positrons implanted at $\overline{z}\approx 9450$ Å.

In the solid phase the *S* parameter for $E=25$ keV does not change appreciably when the temperature increases, indicating that there is no trapping[14] in thermally generated vacancies. Seeger[54] argues that Sn is a metal with narrow ion cores, which preclude vacancy trapping of positrons because the potential well formed at a vacancy is too shallow. The radius of Sn^{4+} is 0.71 Å, which is small compared with the interatomic distances (2.8 and 3.02 Å). The lifetime[14,43] in solid Sn was $\tau\approx 202$ ps, and no trapping was observed at thermally generated vacancies. Dedoussis *et al.*[60] later found a small increase in the lifetime before melting, which they attribute to trapping by thermally generated vacancies. We did not find an increase in the *S* parameter below the melting temperature within the error of the measurement. At the melting point, there is a $\approx$2% increase in the *S* parameter, which indicates positron trapping. Early angular correlation studies[14,59] also indicated vacancy trapping in liquid Sn. We found no published experimental values for the lifetime in liquid Sn.

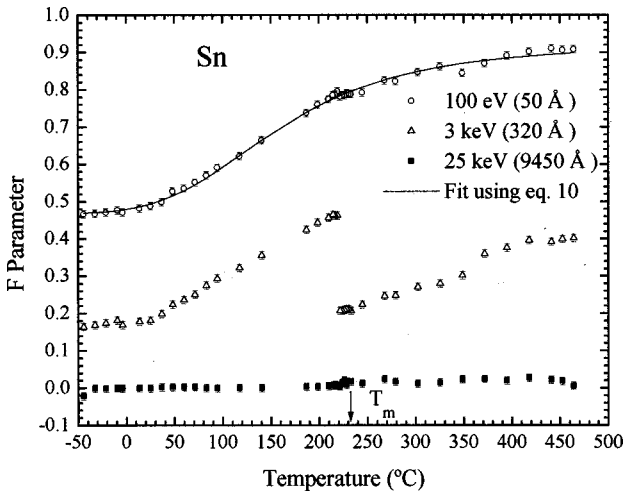

FIG. 9. Positronium fraction for Sn, for the same incident energies as in Fig. 8. No change in Ps fraction is observed at the melting point; see discussion in text.

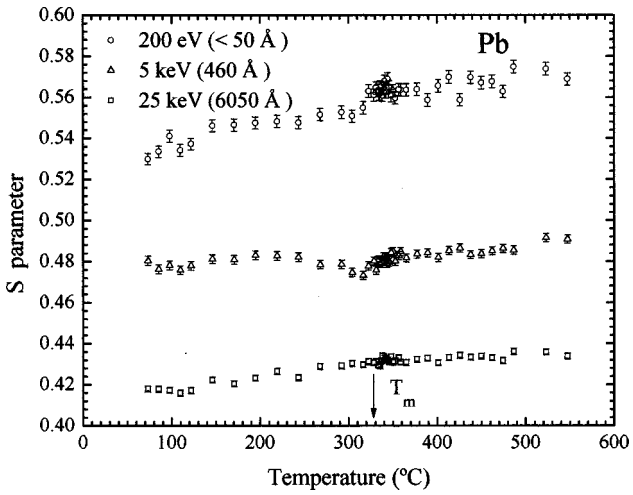

FIG. 10. Experimental S parameter data for Pb plotted against temperature. The top curve ($E=200$ eV) corresponds to $\bar{z}<50$ Å, the second curve ($E=5$ keV) corresponds to $\bar{z}\approx 460$ Å, and the third curve ($E=25$ keV) is for $\bar{z}\approx 6050$ Å.

The S parameter curve at $E=100$ eV in Fig. 8 ($\bar{z}<320$ Å) does not change significantly at the melting point. The small jump most likely reflects changes in the surface geometry. There is a continuous increase in S_s with temperature (even after melting) that is associated with thermal Ps desorption. Figure 9 shows the Ps fraction as function of temperature for the same incident energies as Fig. 8. It can be seen that desorption continues in the liquid phase.

Upon melting, no difference is seen in Ps formation (curve for $E=100$ eV). The electronic density of states (DOS) for β-Sn on the average does not differ much from the liquid DOS.[74] However, the DOS for α-Sn has a minimum at the Fermi energy that is not seen in liquid Sn.[74] Thus measurements of Ps formation across the melting point for α-Sn should yield an increase in the Ps fraction. In our measurements, polycrystalline Sn was used, a mixture of α-Sn and β-Sn, which may be the reason that we do not see a change in Ps formation.

The Ps fraction curve at $E=100$ eV in Fig. 9 can be fitted with Eq. (10); the resulting values are $E_a=0.23(0.01)$ eV, $F_e=0.467(0.004)$, $f_{ts}=0.47(0.01)$, and $\Gamma/\lambda=5(1)\times 10^2$ (see Table III). The solid line shows the fitted results. Using Eq. (9) and the value of the electron work function[51] for Sn, $\phi_-=4.4$ eV, the positron binding energy is $E_b=2.63(0.01)$ eV, which is very close to the theoretical value of $E_b=2.5$ eV.[52]

Jean *et al.*[61] found the activation energy of Ps in Sn to be $E_a=0.38(0.02)$ eV, which is 50% higher than our values. However, their measurements were made below the melting point, and our results show that Ps desorption continues in the liquid phase. This difference could introduce an error in their calibration of Ps fraction at low incident energies (R_1), giving an incorrect value in their fits of the activation energy of Ps. In addition, the difference in E_a could result from its dependence on the crystallographic face. Jean *et al.*[61] used crystalline Sn(110), while our measurements were made with polycrystalline Sn. Differences of 25% have been observed for E_a in different faces of Ag.[6] These effects could account for the 50% difference in the activation energy.

2. Measurements of S and F for Pb and In as a function of temperature

a. Lead. Lead has a low melting point of 327.5 °C, and its vapor pressure at the melting point is $\approx 6.5\times 10^{-9}$ torr. Its density is 11.4 g/cm^3 at room temperature, and it expands 3.5% upon melting.

Pb has been studied with angular correlation,[15,62] lifetime,[63] and positronium time-of-flight[64] techniques. Lifetime[63] studies showed trapping of positrons in thermally generated vacancies, starting from ≈150 °C and reaching saturation close to the melting point. Angular correlation studies[15] in bulk Pb showed similar behavior. Upon melting, an increase in the coincidence count rate at the peak of the angular correlation curve (this is equivalent to the S parameter) shows that the nature of the traps change. It is not clear if this change is related to an expansion of their size or the appearance of a new kind of trap.

Figure 10 shows the S parameter as function of temperature in Pb. As in the other metals, the three curves correspond to positrons implanted at $\bar{z}<50$ Å ($E=200$ eV), at $\bar{z}\approx 460$ Å ($E=5$ keV), and at $\bar{z}\approx 6050$ Å ($E=25$ keV). A small increase is seen in the S parameter curve for $E=200$ eV, which could be due to thermal desorption of the small fraction of positrons that are trapped at the surface. It could be also due to a change in the characteristics of the surface trap. Time-of-flight experiments[64] showed that the positronium work function is negative, so that most positrons reaching the surface form positronium at all temperatures. This conclusion was confirmed by our measurements of the Ps fraction at $E=200$ eV in Fig. 11 that shows a high positronium fraction at all temperatures. This curve also shows a small decrease in Ps fraction at the melting point. However, the electronic DOS in liquid Pb (Ref. 74) increases at ~2 eV below the Fermi energy E_F and decreases at ~4 eV below E_F; so it is difficult to determine the effect of the change in the DOS.

The curve at $E=25$ keV in Fig. 10 shows a small increase starting at 150 °C, reflecting the onset of trapping in thermally generated vacancies. Trifthäuser's results[15] show an

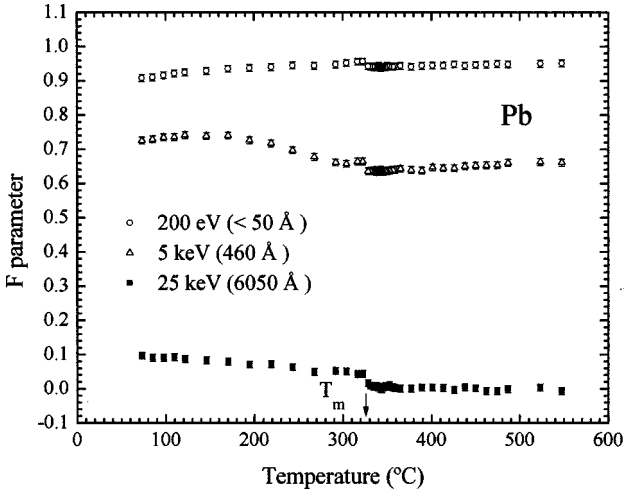

FIG. 11. Experimental values of the positronium fraction for Pb, for the same incident energies as Fig. 10. A small decrease is seen upon melting in the curve for $E=200$ eV.

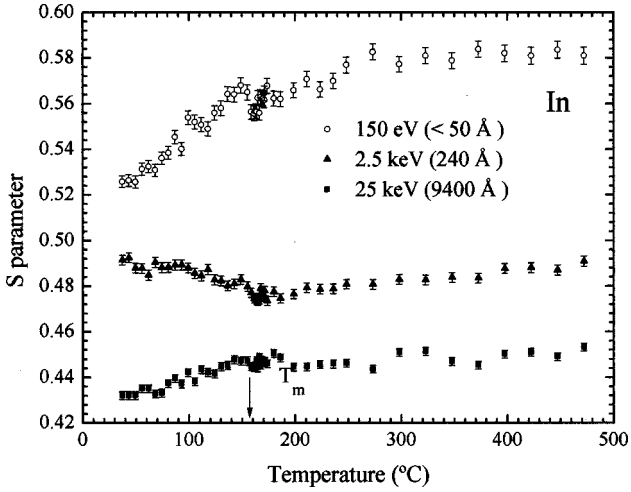

FIG. 12. S parameter curves in solid and liquid In for three implantation depths: $\overline{z}<50$ Å ($E=150$ eV), $\overline{z}\approx 240$ Å ($E=2.5$ keV), and $\overline{z}\approx 9400$ Å ($E=25$ keV).

appreciable increase in the angular correlation curve at the melting point. We do not observe such a large difference because our resolution function is wider than in angular correlation measurements. The formation ~4% of Ps (seen in Fig. 11, for $E=25$ keV) is not enough to change the value of the S parameter below the melting point.

The S parameter results at $E=5$ keV in Fig. 10 show that the fraction annihilating in the bulk and the fraction annihilating at the surface are unchanged upon melting, indicating that the diffusion length is very similar below and above the melting point.

The positronium fraction curve at low incident energy ($E=200$ eV in Fig. 11) shows a small decrease upon melting that can reflect a decrease in the density of electron states.[74] The formation energy of positronium, E_a, and the binding energy of positrons to the surface potential, E_b, cannot be calculated because only a very small percentage of positrons remain at the surface to be later thermally desorbed as positronium. This small fraction does not allow fitting with Eq. (10).

b. Indium. In has a low melting point $T_m=156.6\,^{\circ}$C and a vapor pressure at temperatures close to the melting point of 1×10^{-12} torr. Thus In can be studied over a wide range of temperatures under UHV conditions. Its density is 7.31 g/cm^3. Upon melting, its volume increases by 2.7%. Indium has been studied with angular correlation[15,62] and lifetime techniques.[7,13,55] As with Pb, an increase in the lifetime indicates trapping in thermally generated vacancies. Upon melting, the coincidence count rate of the angular correlation curve increases,[15] suggesting that the size or type of the trapping centers changes or that the fraction of trapped positrons increases.[15]

The curve for $E=150$ eV in Fig. 12 corresponds to an implantation depth of $\overline{z}<50$ Å, the curve at $E=2.5$ keV is for $\overline{z}\approx 240$ Å, and the curve at $E=25$ keV is for $\overline{z}\approx 9400$ Å. At $E=150$ eV, the S parameter increases with temperature and is associated with thermal desorption of positronium. Figure 13 shows the positronium fraction for the same incident energies as Fig. 12. The curve at $E=150$ eV shows that Ps starts to be thermally desorbed at ≈20 °C. As in the other metals, the S parameter does not change appreciably upon melting (except for a jump due to change in the geometry of the sample or release of impurities from the surface).

From the data at $E=150$ eV in Fig. 13, we can see that the Ps fraction decreases slightly upon melting. Also, the electronic density of states decreases slightly at ~1 eV below the Fermi energy[47] upon melting; so there are fewer electrons with energy close to the Fermi energy available to form Ps. These effects may explain the decrease in the Ps fraction.

The S parameter curve for $E=2.5$ keV in Fig. 12 decreases in the solid phase with temperature, indicating that the fraction of positrons that reach the surface decreases as the temperature increases. This effect also indicates that the diffusion length decreases. This is very clearly seen in the measurements of the Ps fraction in Fig. 13, where the curve for $E=2.5$ keV shows a rapid decrease in Ps fraction.

The S parameter curve at $E=25$ keV and below the melting point in Fig. 12 corresponds to positrons annihilating

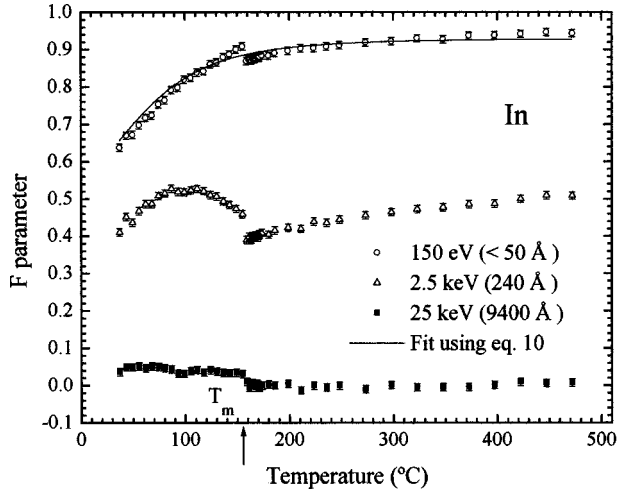

FIG. 13. Positronium fraction curves in In at the same three different implantation depths as shown in Fig. 12. The decrease in Ps fraction for $\overline{z}<50$ Å is consistent with a small decrease (Ref. 47) in the DOS at 1 eV below E_F.

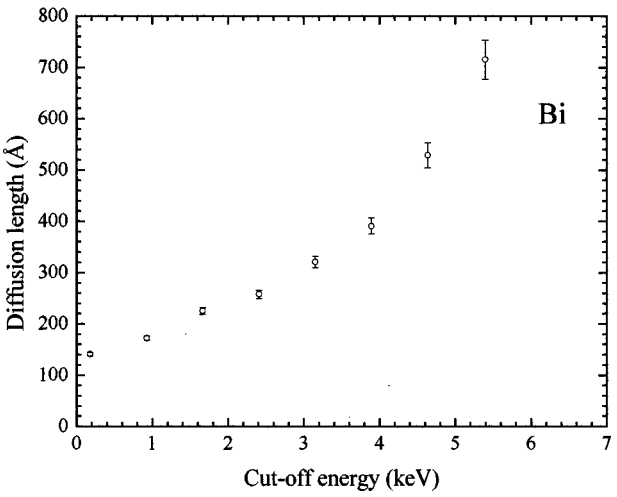

FIG. 14. Fits to the S parameter data in Bi at $T=408\,^{\circ}\mathrm{C}$. The diffusion length was calculated with VEPFTT, selecting different cut-off energies to start the fit.

primarily in the bulk. At this implantation energy there is a small fraction of positrons that can diffuse back to the surface and annihilate there. This effect can be seen more clearly in Fig. 13. The positronium fraction even at $E=25\,\mathrm{keV}$ is about 2–3 %, just below the melting point.

Figure 12 also shows a small increase below the melting point in S for $E=25\,\mathrm{keV}$ when the temperature increases. This effect, seen before with angular correlation techniques,[14,15] shows that positrons become trapped in thermally generated vacancies. An early study[7] of lifetime in solid In revealed an increase from ≈200 ps at 25 °C, to 250 ps at 150 °C (just below the melting point). Crisp *et al.*[13] found that the bulk lifetime in In was $\tau_b=182\,\mathrm{ps}$. Close to the melting point, they found a vacancy lifetime of $\tau_v=240\,\mathrm{ps}$. Kishimoto and Tanigawa[55] also showed that the lifetime increases as the temperature increases from 220 ps at 25 °C to 260 ps at 130 °C. Very close to the melting point, there was an additional fast rise in the lifetime, which they attributed to formation of divacancies or to the presence of impurities in In.

Although the lifetime values from different experiments differ, they all show an increase that can be attributed to positron trapping in thermally generated vacancies. The change in angular correlation[15] below T_m and the small change upon melting indicate that positrons annihilate from trapping sites in the melt. The change that they observed upon melting is probably due to a variation in the kind of traps.[15]

The S parameter for $E=25\,\mathrm{keV}$ (Fig. 12) does not change at T_m. We cannot observe a difference between solid and liquid In with the S parameter because of the large experimental error.

The solid line in Fig. 13 shows a fit to the positronium fraction curve using Eq. (10), to obtain the activation energy of Ps: $E_a=0.25(0.01)\,\mathrm{eV}$, $F_0=0.47(0.03)$, $f_{ts}=0.46(0.02)$, and $\Gamma/\lambda=8(2)\times10^3$. The electron work-function[51] in In is $\phi_+=3.8\,\mathrm{eV}$; therefore, from Eq. (9), the binding energy of positrons to the surface state is $E_b=3.25(0.01)\,\mathrm{eV}$. Nieminen and Hodges[52] calculated the positron binding energy to be $E_b=2.4\,\mathrm{eV}$ and the positron work function to be $\phi_+=2.6\,\mathrm{eV}$. They predicted that a surface state cannot exist in In. But our results in Fig. 13 show the existence of a surface state in liquid and solid In.

B. Diffusion length

1. Analysis of diffusion data

For all metals we investigated, the diffusion length in the solid phase decreases with increasing temperature, decreases or remains constant on melting, and then increases with further increasing temperature in the melt. As in Sec. IV A, our results are discussed separately according to the state of the positron in the solid phase below the melting point. The first group is the metals, Ga, Bi, Sn, and Na where positrons do not get trapped in thermally generated vacancies; the second group is Pb and In in which positrons are trapped at vacancies in the solid phase.

The diffusion length was obtained by solving numerically Eq. (3) and fitting it to the data. The routine used was VEPFIT, developed by van Veen *et al.*[41]; the fitted parameters were the fraction F_s of positrons reaching the surface, the diffusion length L_+, the S parameter in the surface S_s, and the S parameter in the bulk S_M. The parameters defining the Makhov profile, m and n, were fixed for each metal, following Schultz and Lynn.[6]

The F and S parameters were measured versus energy for several temperatures of interest. The model, described in Sec. II, was fitted with VEPFIT to the positronium fraction data, calibrated according to the procedure described in Sec. II D, to obtain the fraction F_0. The S parameter arising from Ps annihilation (S_{Ps}) was extrapolated from the curves of S as function of energy. At high temperatures, with low incident energy, and in a clean surface, more than 90% of the contribution to the S parameter will come from parapositronium. The value obtained was $S_{\mathrm{Ps}}=0.62$, extrapolated at $E=0$

Subsequently, the S parameter data was fitted with Eq. (5), using the estimated S_{Ps} and the deduced F_0 as an input to the program. These values are included in the calibration factor Ω [Eq. (7)]. The diffusion length, obtained from fits to the F parameter, is not reliable because accurate calibration factors R_0, R_1, and P_1/P_0 cannot be obtained. These parameters are also very dependent on the condition of the surface, which can change during the experiment. Therefore, we show only the diffusion length obtained from fits to the S parameter.

To estimate the error in the fit due to the contribution from nonthermal positrons, a grid was placed in front of the sample and biased to +50 and −50 V. For each bias, the S parameter was measured as function of energy, using the same energies as those used to measure the diffusion length. With a bias of +50 V, any nonthermal positron that is reemitted from the sample will return to it. These positrons have less energy than the incident positrons, and they will tend to increase the value of the S at low incident energies. A fit to these data will give a smaller diffusion length. With a bias of −50 V, nonthermal positrons are removed from the sample and a fit to these data will give a higher diffusion length. The difference in the diffusion length between the +50 and −50 V will give an estimate of the error.

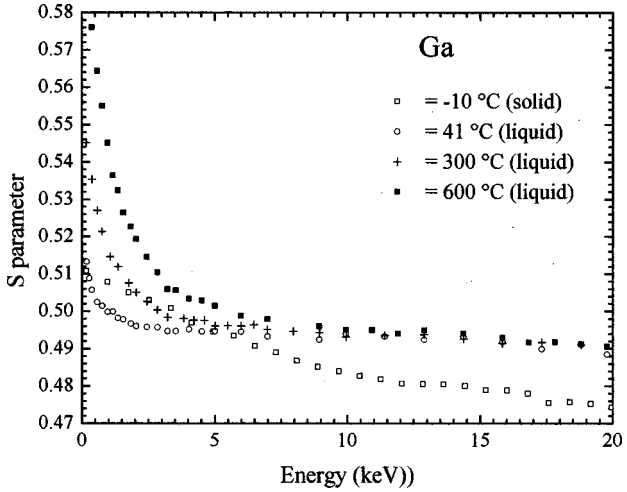

FIG. 15. *S* parameter in Ga as function of incident energy for different temperatures. These curves were fitted to obtain the diffusion length vs temperature.

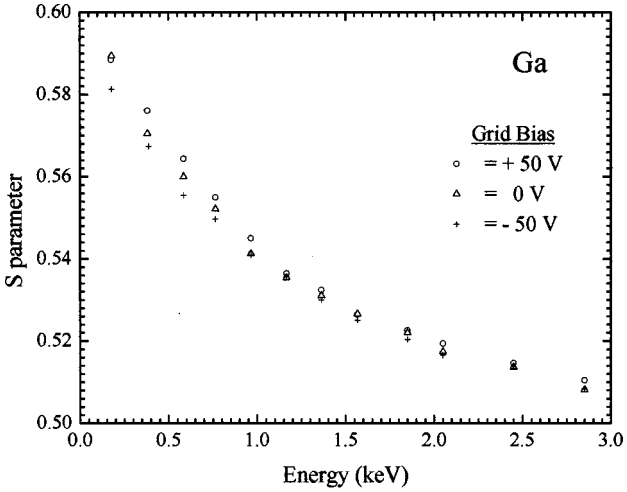

FIG. 16. *S* parameter for $T=600\,^{\circ}\mathrm{C}$, with a grid in front of the sample biased at three different voltages. These data were used to estimate the experimental error from nonthermal positrons in the fitting routine.

Huomo *et al.*[40] proposed another method to analyze the *S* and *F* parameters when nonthermal positrons are present. They chose a minimum implantation energy for the data analysis and assumed that *S* is a nearly linear function of *F*. The deviation from linearity is mainly associated with nonthermal positrons reaching the surface. Also, they considered only energies above that where such deviation occurs. However, the assumption of linear *F* with *S* is only valid for $f_0 < 0.3$. One problem with the method of Huomo *et al.* is that when the energy chosen to start the fit is increased, the resulting diffusion length increases monotonically. Consequently, if the wrong minimum energy is chosen, the diffusion lengths will not have an upper bound. To illustrate this point, Fig. 14 shows the resulting diffusion length when different starting energies are used (the data were generated from fits to the *S* parameter data in Bi at 408 °C).

2. Measurements of diffusion length in Ga, Bi, Sn, and Na

a. Gallium. The data used to calculate the diffusion length were taken at a fixed temperature, varying the energy from 100 eV to 20 keV. More points were measured from 100 eV to 2 keV because the changes in *S* or *F* parameters were larger here than at high incident energies. Figure 15 shows measurements of *S* as function of energy for different temperatures.

The fits were performed with the fitting routine VEPFIT. The values used for *m* and *n* were 2 and 1.4, respectively. The second value was used because preliminary Monte Carlo simulations[28] of the stopping profile show $n \approx 1.4$ for Ga. The error in the fit introduced by nonthermal positrons escaping the sample is estimated using the method explained in Sec. IV B 1. Data with a grid in front of the sample at $+50$, -50, and 0 V are shown in Fig. 16. In all cases the error from this effect was less than the error obtained from the fitting routine.

The results of the fitting are shown in Fig. 17. The error bars come from the fitting routine and are quoted in parentheses in the text. Below the melting point, the diffusion length is $L_+ = 1200(100)$ Å. This large diffusion length confirms the results obtained previously,[12,65] that below the melting point positrons are in a Bloch-like state and the diffusion length is long. The diffusion coefficient D_+ can be calculated from the definition given in Sec. II E, using the lifetime in solid Ga given by Segers *et al.*,[44] $\tau = 193(5)$ ps. The result is $D_+ = 0.75(0.06)\ \mathrm{cm}^2/\mathrm{s}$, larger than the theoretical value obtained by Bergersen *et al.*[17] of $D_+ = 0.4\ \mathrm{cm}^2/\mathrm{s}$.

Upon melting, the diffusion length drops to $L_+ = 60(5)$ Å, a change of almost two orders of magnitude. This large drop is consistent with the explanation that the positron changes from a Bloch-like state to a trapped state. As the temperature is increased further, there is an increase in the diffusion length that starts at $\approx 150\,^{\circ}\mathrm{C}$.

The following scenario may explain the increase in the diffusion length in the liquid phase. The time it takes to trap a positron[4] in a vacancy or defect is about 10^{-15} s, which is much faster than the time scale for motion of ions in liquids[1,2] ($\sim 10^{-12}$ s). Thus the positron can be seen as in-

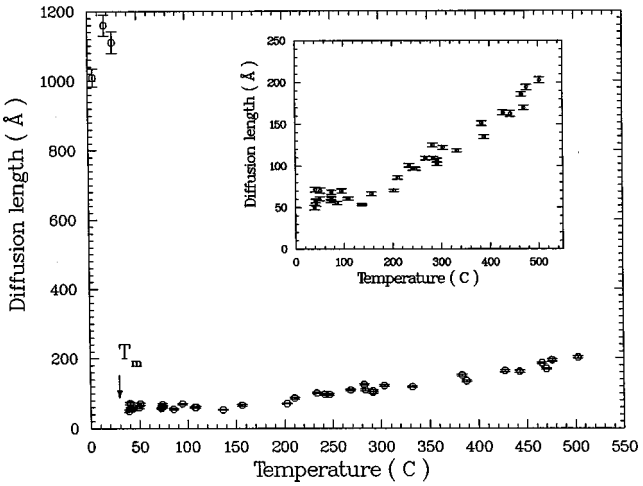

FIG. 17. Diffusion length results for Ga as function of temperature. A large drop is observed on melting. The inset shows the rapid increase of the diffusion length in the liquid phase. The error bars shown are statistical estimates from the fitting routine.

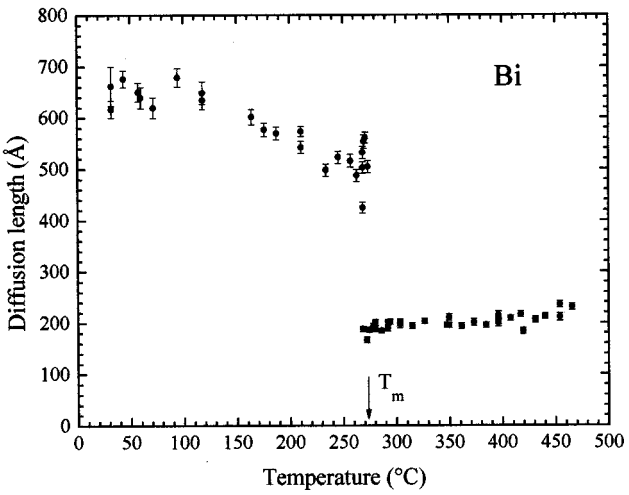

FIG. 18. Diffusion length results in solid and liquid Bi plotted vs temperature. The large drop in the diffusion length at the melting point can be easily seen.

teracting with an almost static array of ions and can adjust to any ionic displacement. Density fluctuations on a time scale of 10^{-12} s could produce potential wells strong enough to trap positrons. These traps could later disappear (or change in size), forcing the positron to jump to a nearby fluctuation. Thus positron diffusion in liquid Ga can be seen as a hopping motion between traps, with trapping and detrapping happening many times during the lifetime of the positron ($\sim 10^{-10}$ s). As the temperature increases, the frequency of these fluctuations would increase, increasing the hopping motion and the diffusion length. Thermally activated detrapping alone is unlikely to explain the increase in the diffusion length because the thermal energy of the positron is much less than its binding energy to the trap.[9]

Such fluctuations can explain the decrease in lifetime with higher temperatures[12] in Ga, because the lifetime will be given by the weighted average of the lifetime in the traps (260 ps) and the lifetime in the bulk (193 ps).

The trapping scenario in liquid Ga is similar to the high-m^+ state described by Seeger,[23] where positrons couple to acoustic phonons to create acoustic e^+ polarons. In this state, the positron wave function is strongly localized in the interstices between atoms, and its motion is well described by hopping.

b. Bismuth. Figure 18 shows the diffusion lengths for Bi following the same fitting procedure as for Ga. At room temperature, $L_+ \approx 650$ Å; however, this value may be smaller than the real value because of systematic errors in the fitting routine. VEPFIT assumes that, at high incident energies, all positrons annihilate in the bulk. However, the maximum energy reached by the beam is 25 keV, at which energy some positrons still can reach the surface. Thus $S(E=25\,\text{keV})$ is different than S_M and the fitted diffusion length will be low. The error bars in the solid phase are larger than in the liquid because the dynamic range of the S parameter used to fit the diffusion length is larger in the liquid. At 31 °C, the S parameter varies from ~ 0.528 at $E=100$ eV to ~ 0.50 at $E=25$ keV, a 5% change, while at 276 °C, the change is from $S \sim 0.603$ to $S \sim 0.50$, a 20% change.

The theoretical value of the diffusion length can be obtained from the model given by Bergersen *et al.*[17] At 25 °C, they obtain $D_+ = 0.33\,\text{cm}^2/\text{s}$ (using $E_d = -\frac{2}{3}E_F = -6.6$ eV and $m^* = 1.8m_e$) and the bulk lifetime is[56] $\tau = 258$ ps. Thus $L_+ = 920$ Å, which is higher than our experimental value. This discrepancy may be due to overestimating the asymptotic value of S in the experimental data.

Diffusion of positrons in solid metals is dominated by phonon scattering,[17] and at temperatures above ~ 25 K the temperature dependence is expected to be $D(T) = D_0/T^\eta$, with $\eta = 1/2$ and D_0 a constant. Using the diffusion length as dependent variable, this equation is equivalent to $L_+(T) = L_0/T^{\eta/2}$. There have been experimental results[6] that show higher values for η for several metals; so it is interesting to calculate it for Bi. The temperature range of our diffusion data for Bi below the melting point is large enough to allow a nonlinear fitting using the previous equation. The results is $\eta = 0.9(1)$. This value is clearly higher than 1/2, which is expected by the theory.

Close to the melting point, our fitted value of $L_+ \approx 500$ Å for solid Bi, which may still be lower than the actual length. The theoretical value for the diffusion length calculated according to Ref. 17 is $L_+ = 790$ Å at 270 °C. Upon melting, L_+ drops to ≈ 190 Å. As mentioned in Sec. IV B 1, measurements were performed to estimate the error in the calculation of the diffusion length arising from nonthermal positron emission. The experimental error from measurements of the S parameter versus energy with a grid in front of the sample is ± 40 Å in the solid and ± 20 Å in the liquid.

In liquid Bi, at high incident energies, all positrons annihilate in the bulk (as seen in Fig. 5 for positrons implanted deep into the sample at $E=25$ keV) and the calculated diffusion length should not underestimated.

Diffusion in liquid Bi resembles the low-m^+ state described by Seeger.[23] In this state, Bloch wave description of the positrons also seems to be appropriate.

c. Sodium. As was mentioned in the discussion of S and F versus temperature, the S parameter in Na has only a weak dependence with the incident energy. This effect can be seen in Fig. 19, that shows no appreciable difference between positrons implanted close to surface ($E \approx 100$ eV) and positrons implanted deep into the bulk ($E=25$ keV) because all annihilate in the bulk. The small difference between the curves is associated with nonthermal positrons or positronium. The measured S parameter will have a large component from S_{bulk} and a small component from nonthermal positron and positronium annihilation. In consequence, it is not possible to extract the diffusion length from the experimental data.

The positronium fraction versus incident energy is plotted in Fig. 20; there is a rapid decrease from $E=100$ eV to $E=1$ keV. Theoretical calculations[34] show that no Ps should be formed at the surface. The F parameter seen in Fig. 20 at low incident energies is attributed to nonthermal positrons, which have enough energy to overcome the potential step at the surface and leave the sample. Because the mean free path for nonthermal positrons is short,[34] they can reach the surface only if the mean implantation depth is small.[40] Thus the number of nonthermal positrons reaching the surface decreases rapidly as the incident energy is increased.

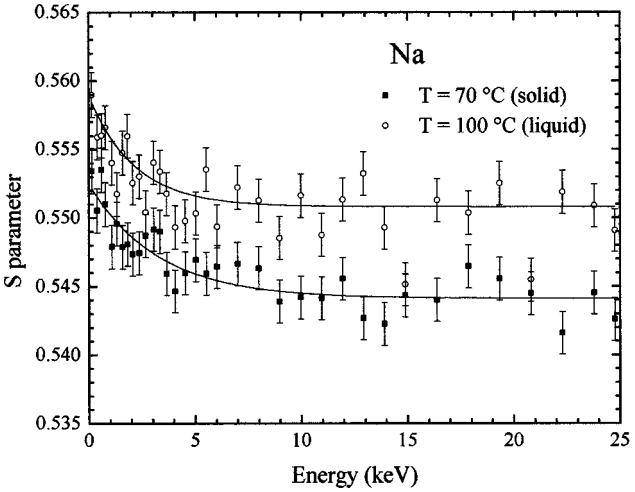

FIG. 19. *S* parameter in solid (70 °C) and liquid Na (100 °C), plotted as function of the incident energy. There is little change between low and high incident energies. The higher *S* parameter at low energies is associated with nonthermal Ps formation. The solid lines are a guide to the eye.

Evidence that the data in Fig. 20 cannot arise from thermal positronium formation is the following. We have plotted in this figure the theoretical fraction of Ps that would be generated by thermal positrons reaching the surface. This fraction was calculated by inserting the theoretical value[53] of the diffusion length at room temperature ($L_+ \approx 1800$ Å) into the diffusion equation; then, the number of thermal positrons that return to the surface can be obtained for any given energy. This fraction is shown in Fig. 20 (solid line); along with the measured Ps fraction, we have set $F_0 \approx 0.09$ (also from Fig. 20). It can be seen that the measured positronium fraction decreases faster with energy than the theoretical fraction. Another evidence that there is no Ps formation comes from the small difference in *S* the parameter at low

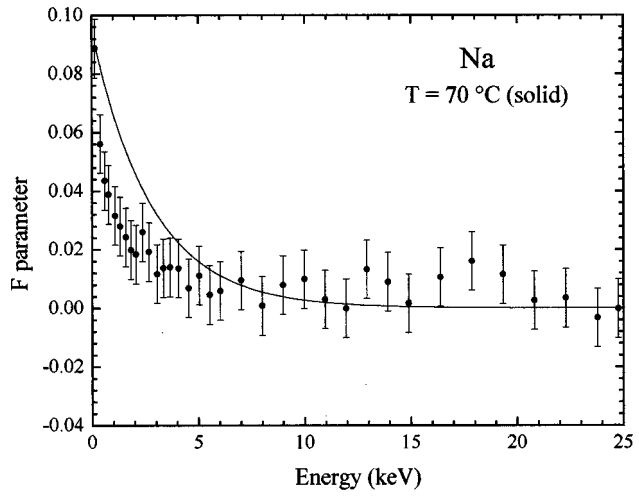

FIG. 20. Positronium fraction in Na, as function of the incident energy. A rapid decrease can be seen as the incident energy increases. The solid line is the amount of Ps that would be formed from thermal positrons reaching the surface. The difference with the experimental data is an indication that there is only nonthermal Ps formation at the surface.

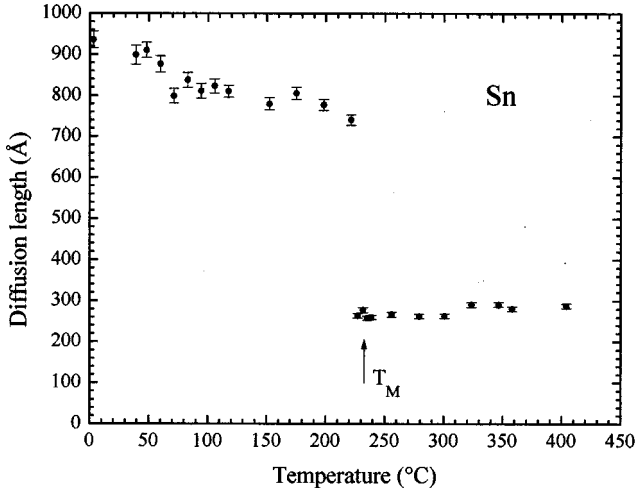

FIG. 21. Diffusion length results for Sn above and below the melting point as a function of the temperature.

and high incident energies (~1%). All other metals have a larger difference (5–17 %).

d. Tin. Figure 21 shows the diffusion length versus temperature for Sn, which is similar to that of Bi. Below the melting point, the diffusion length decreases slowly with increasing temperature. In both metals, positrons are in a Bloch-like state in the solid phase. Accordingly, the diffusion length is expected[17] to decrease as $\approx T^{-1/4}$ because phonon scattering is the dominant interaction between positrons and the metal. At temperatures below ≈100 °C, the diffusion length is not accurate because the energy range of the beam is not high enough to reach the bulk value of *S*.

The theoretical value for the diffusion length can be calculated from Ref. 17. At 30 °C, we obtain $D_+ = 1.12\ \mathrm{cm}^2/\mathrm{s}$ ($E_d = -2/3E_F = 6.7$ eV, $m^* = 1.8m_e$, and the bulk lifetime[43] is $\tau = 202$ ps. Thus the theoretical value of the diffusion length is $L_+ \approx 1500$ Å, which is much larger than the fitted diffusion length in Fig. 21, $L_+ \approx 950$ Å at $T = 30$ °C. As in Bi, overestimating the asymptotic value of *S* in the fits leads to smaller values for L_+.

As was the case for Bi, the temperature range of our diffusion data for Sn below the melting point is large enough to allow a nonlinear fit. The result is $\eta = 0.76 \pm 0.10$, which is higher than the theoretical value.[17]

Just below the melting point, $L_+ = 750(50)$ Å; the theoretical value at this temperature is $L_+ \approx 1100$ Å. Upon melting, the diffusion length drops to ≈260(20) Å. The error in our values of L_+ was calculated from the fitting routine. In Sn, the drop observed at the melting point can be explained by vacancy trapping or increased scattering with the more mobile ions in liquid Sn.

Early Ps fraction measurements with a positron beam[61] showed that E_0 decreased as the temperature increased (E_0 is related to the diffusion length by[8] $E_0 = L_+/A$). Jean *et al.*[61] attributed this decrease to trapping in thermally generated vacancies. However, they used incident energies only up to 5 keV, which may be too low to extract the correct E_0. Their diffusion length was $L_+ \approx 300$ Å, which is smaller than our results.

There is a slight increase in the diffusion length with increasing temperature which resembles the Bloch-wave state described by Seeger.[23]

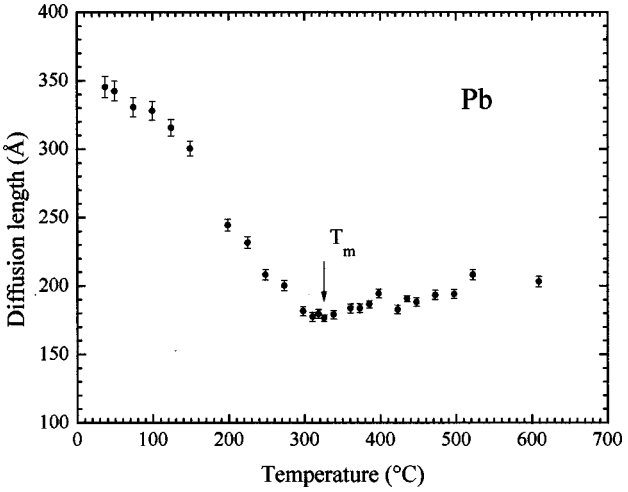

FIG. 22. Diffusion length in Pb from fits to the *S* parameter. No change in the diffusion length at the melting point (indicated with an arrow) is observed within the experimental error. The rapid decrease with temperature in the solid phase is due to positron trapping in thermally generated defects.

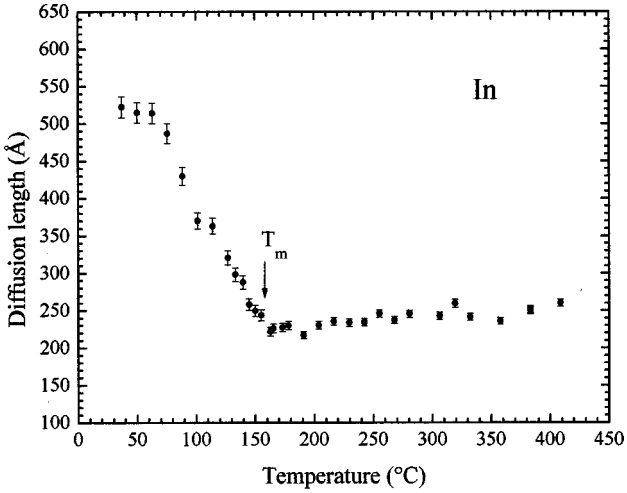

FIG. 23. Diffusion length in In as function of the temperature, obtained from fits to the *S* parameter. As in Pb, no change in the diffusion length is observed at the melting point.

3. Measurements of diffusion length in Pb and In

Pb and In show a pronounced trapping effect below the melting point, as was evidenced by S_M and also by the diffusion length. A rapid decrease in diffusion length occurs when positrons begin to get trapped at thermally generated vacancies. Upon melting, the trapping sites may change, but the diffusion characteristics are not significantly affected, and there is only a small decrease in the diffusion length.

a. Lead. The results from fits to the *S* data are shown in Fig. 22, where the diffusion length is plotted versus temperature.

At room temperature, $L_+ \approx 350\,\text{Å}$. However, this value may not be accurate because, at high incident energies and low temperatures, some positrons can still reach the surface. The theoretical value for the diffusion length[53] is $L_+ = 1200\,\text{Å}$, using $\tau = 168\,\text{ps}$ for the bulk lifetime[63] in solid Pb. This is an order of magnitude larger than the fitted result.

As the temperature increases, the diffusion length decreases rapidly in the solid phase because of the combined effect of phonon scattering and thermal vacancy trapping. Just below the melting point, $L_+ \approx 180(20)$ Å and diffusion is dominated by trapping. Upon melting, there was no change in the diffusion length, consistent with the assumption that all positrons are trapped in the solid phase below the melting point. An increase in the concentration of traps or decrease in the electronic density of states[74] does not seem to affect the diffusion length upon melting.

In contrast to any of the previous metals, we did not observe nonthermal positrons or Ps being emitted from the sample. The positronium work function is negative and there is a high fraction of Ps at all temperatures. Thus nonthermal Ps cannot be distinguished from thermal Ps. As the temperature increases, the diffusion length increases slightly, as observed for all metals.

b. Indium. Previous studies[15] with In show a pronounced trapping effect in the solid phase as the temperature is increased. Therefore, as in Pb, the diffusion length in the solid phase varies strongly with temperature.

Figure 23 shows the results of the fit to the *S* parameter. At room temperature, $L_+ \approx 530\,\text{Å}$. As in Pb, Bi, and Sn, this value may underestimate the real value. At room temperature, the bulk lifetime is $\tau = 220\,\text{ps}$,[55] and $D_+ = 0.13\,\text{cm}^2/\text{s}$. The theoretical diffusion coefficient can be obtained from Ref. 17. At $T = 27\,^\circ\text{C}$, $D_+ = 0.4\,\text{cm}^2/\text{s}$, which is larger than the our fitted results.

The rapid decrease in the diffusion length from 50 °C to the melting point is attributed to trapping in thermally generated vacancies.[13] This decrease is much faster than the decrease in metals with no vacancy trapping (Ga, Bi, or Sn) in the solid phase. Close to the melting point, the diffusion length is $L_+ \approx 245(20)$ Å (Fig. 24). The lifetime at this temperature[55] in solid In is $\tau = 280\,\text{ps}$. Thus the diffusion coefficient is $D_+ = 0.021\,\text{cm}^2/\text{s}$.

As with Pb, nonthermal positrons do not play a role in calculating diffusion length. Measurements of the *S* parameter with a grid in front of the sample do not show any difference for different bias voltages.

4. Comparison of diffusion data to prediction of e^+-polaron model

Recently, Seeger[23] has published an analysis of our diffusion length measurements[16] for Ga and Bi, based on a model in which positrons couple to acoustic phonons to create acoustic e^+-polaron states. The model predicts two types of polarons, designated according to effective mass as low-m^+ states and high-m^+ states. In a low-e^+ state, a Bloch-wave description of the positron motion is valid, but the effective mass may exceed the positron mass by several orders of magnitude because the positron's motion is accompanied by displacement of ions. In a high-m^+ state, the positron is strongly localized interstitially, and its motion is best described by hopping. The high-m^+ state would correspond to the hopping motion picture described in our previous paper.[16]

Seeger has made clear predictions of the behavior of positron diffusivity across the melting transition and as a function of temperature above the melting point for the two types

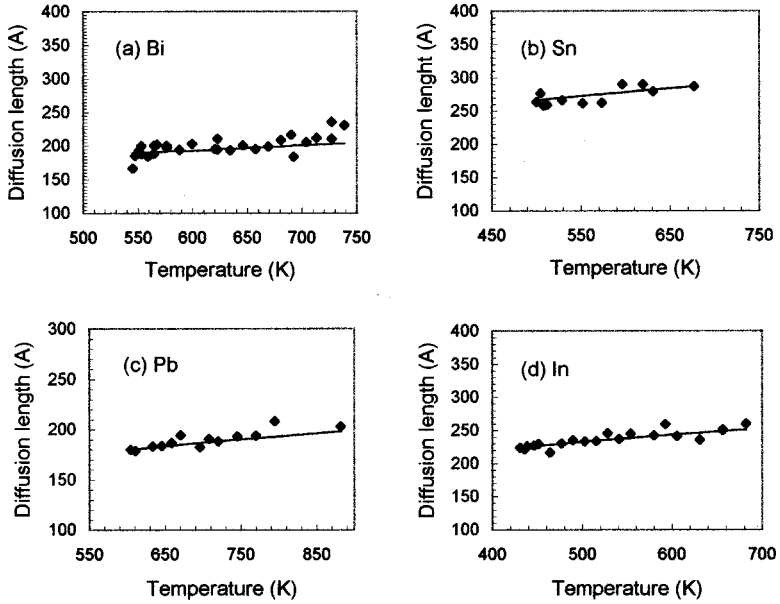

FIG. 24. Fits to the temperature dependence of the positron diffusion length using the low-m^+ state model (Ref. 23) in four metals studied. (a) Diffusion length in Bi. The solid line is a fit using Eq. (12). Diffusion length in (b) Sn, (c) Pb, and (d) In.

of polarons. The prediction of the change in diffusivity at the melting transition assumes that the solid does not contain thermally generated vacancies. For systems with a low-m^+ state, he predicts a drop in diffusivity at the melting point and a $T^{1/2}$ power temperature dependence above the melt. For systems with a high-m^+ state, he predicts a larger drop in diffusivity at the melting point and an Arhenius-type temperature dependence in the liquid. He shows that our data for Ga are well described by the high-m^+ case, while the data for Bi fit the low-m^+ case.

Examination of our diffusion data for Sn, Pb, and In shows that the Sn data are very similar to the Bi data, pointing to a low-m^+ state in liquid Sn. For Pb and In, thermal vacancy formation in the solid prevents application of the model to the behavior at the phase transitions. However, the temperature dependence within the liquid is again similar to that of Bi, indicating a low-m^+ state.

Following Seeger's work, we can estimate the magnitude of the effective mass of the positron in the low-m^+ state. The effective mass can be calculated from

$$D^+ \approx l\left(\frac{3k_BT}{m^+}\right)^{1/2}, \tag{11}$$

where $l=\langle v^2\tau_m^2\rangle^{1/2}$ is the mean free path of the positrons, which, in a liquid, can be identified with the interatomic distance.[23] The interatomic distance l_i can be obtained from calculations of the interatomic pair potential in a liquid.[74]

For Sn, the interatomic distance[74] is $l_i \approx 4$ Å, which we can identify with the mean free path of the positrons, l. The diffusion length just above the melting point is $L_+ = 260$ Å, and the positron lifetime τ is 220 ps. Thus the diffusion constant can be obtained from $D_+^2 = L_+^2/\tau$, which for Sn is 3.4×10^{-6} m^2/s. Using Eq. (11), we obtain, for the effective mass in liquid Sn, 2.9×10^{-28} kg. This mass corresponds to $\sim 0.2m_p$ (m_p is the mass of the proton), indicating that the positron is in a low-m^+ state.

For Pb, the interatomic distance[74] is $l_i \approx 3.8$ Å. The diffusion length just above the melting point is $L_+ = 180$ Å, and the positron lifetime τ is 275 ps. Thus the diffusion constant is 1.2×10^{-6} m^2/s. Using Eq. (11), we obtain, for the effective mass in liquid Pb, 1.1×10^{-27} kg ($\sim 0.7m_p$), also in a low-m^+ state.

For In, the interatomic distance[74] is $l_i \approx 4.5$ Å. The diffusion length just above the melting point is $L_+ = 225$ Å, the positron lifetime is $\tau = 260$ ps, and the diffusion constant is 1.95×10^{-6} m^2/s. Thus the effective mass of the positron in liquid In is 0.9×10^{-27} kg ($\sim 0.6m_p$), also in a low-m^+ state.

The temperature dependence of the diffusion length for liquid Bi is rather weak and is described quite well[23] with the low-m^+ polaron state. We have seen in the previous sections that for the other metals under investigation, the temperature dependence is also weak and can also be described using the low-m^+ polaron state. Following Seeger's model, the temperature dependence of the diffusion length is

$$L_+ = L_0 T^{1/4}. \tag{12}$$

We have fitted Eq. (12) to the experimental data using a nonlinear fitting routine with L_0 as a free parameter. The fits results and the experimental data are shown in Fig. 24. The value obtained for L_0 is shown in Table IV, below.

C. Nonthermal-positron effects

The energy loss process of charged particles in a solid or liquid recently has received much attention[66–70] because the analysis of the S and F parameter data strongly depends on a knowledge of the positron implantation profile.[70]

The energy analysis of the reemitted positrons was performed with two parallel grids in front of the sample. The sample was maintained at 30 V, and the grid bias varied from 10 to 50 V. Nonthermal positrons that leave the sample having the normal component of the kinetic energy less than the grid potential return to the metal where they annihilate.

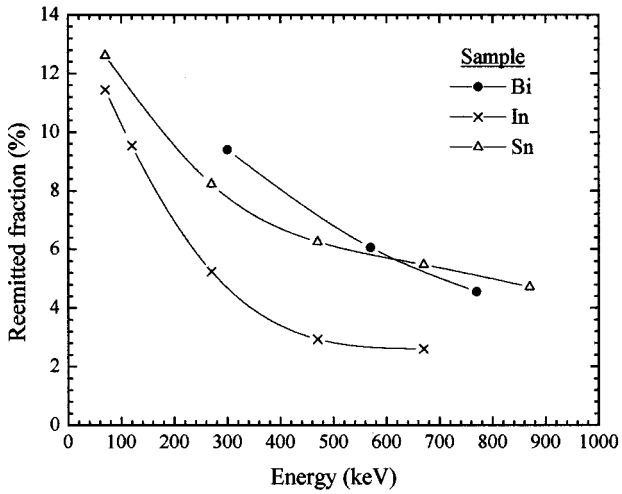

FIG. 25. Fraction of incident positrons reemitted from several metals, plotted against the implantation energy. The rapid decrease reflects the efficient mechanism of energy loss in metals. The solid line is a guide to the eye.

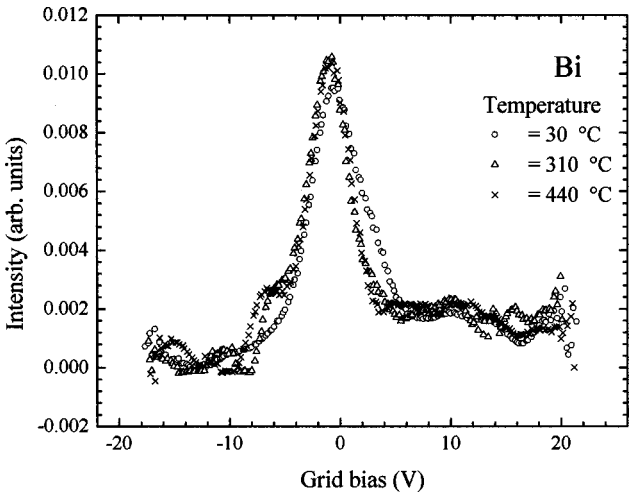

FIG. 26. Differential energy distribution of positrons reemitted from Bi, after being implanted at $E=270\,\mathrm{eV}$, at three different temperatures. $T=310$ and 440 °C corresponds to liquid Bi. The fraction is independent of temperature, showing that there is no trapping of nonthermal positrons in the liquid phase.

Positrons with higher energy pass through the grids and are removed by an $\mathbf{E}\times\mathbf{B}$ energy filter. By changing the grid bias, we can obtain an integral energy spectrum of reemitted nonthermal positrons. The energy spectrum is obtained by differentiating a Gaussian smoothed spectrum (1.1 eV at FWHM). The oscillations in the curves are produced by the smoothing routine.

In all metals studied, the positron work function is positive. Thus the spectra of the reemitted positrons reflect the energy distribution of positrons that have energy greater than ϕ_+.

The energy loss mechanism for positrons in metals is very efficient, and the reemitted fraction strongly depends on the incident energy, as shown in Fig. 25. It can be seen that as the incident energy is increased, the reemitted fraction of positrons decreases very rapidly. Because this fraction is small, the analysis of the diffusion length is not greatly affected by nonthermal positrons.

a. Bismuth. The energy spectra from positrons reemitted from metals with a negative work function should be centered[71] around $E=\phi_+ + \delta E$, where δE is the difference in the contact potentials between the sample and grid in front of the sample. For most metals the contact potential is an order of magnitude smaller than the work function.[72] In addition, it can be expected that after having the sample at high temperatures it would evaporate material over the grids, giving no difference in contact potential.

The energy spectra from positrons reemitted from the surface of Bi is shown in Fig. 26. For positrons implanted at $E=270\,\mathrm{eV}$ and 30 °C, the peak of the energy spectra is centered around $E=0$. This measurement indicates that the positron work function for Bi is smaller than the accuracy of our measurements ($\approx$1 eV)]. To our knowledge, there are no theoretical calculations of the positron work function in Bi. The curves at 310 and 440 °C are measured in liquid Bi; the curve at 30 °C is measured in polycrystalline Bi. As can be seen from the figure, the fraction of reemitted positrons is $\approx$10%, independent of temperature, which indicates that the mechanism of energy loss for positrons with $E>\phi_+$ is independent of temperature or state (solid or liquid). These data also suggest that the implantation profile does not change appreciably upon melting.

Previous studies[25] of nonthermal positron reemission in aluminum found a large decrease in the reemitted fraction when the sample was heated. Above 570 °C, the fraction of reemitted positrons with energies less than 2 eV was reduced. This effect was attributed to the creation of thermal vacancies which trap nonthermal positrons before they can escape. This effect was not observed in liquid or solid Bi.

b. Sodium. Because Na is a very reactive metal, with a high vapor pressure, only data at low temperatures could be obtained. Since its work function is highly positive ($\phi_+ = 4.8\,\mathrm{eV}$), the reemitted fraction from the surface of Na is smaller than in Bi. At $E=70\,\mathrm{eV}$, the fraction was $\approx$7.0%. We measured the reemitted spectra with an implantation energy of $E=70\,\mathrm{eV}$, at 45 and 85 °C (solid Na) and 110 °C (liquid Na). The curves are similar to Bi, and the reemitted fraction is independent of temperature.

c. Tin. The positron work function[52] in Sn is 2.7 eV; therefore, only nonthermal positrons with $E>\phi_+$ can be reemitted. The fraction of incident positrons reemitted at $E=70\,\mathrm{eV}$ from the surface of Sn was $\approx$13.6%. The sample was measured at 31 and 180 °C (solid Sn) and at 240 °C (liquid Sn). As before, the curves for the three temperatures are similar and centered at $E=0\,\mathrm{eV}$.

In solid Sn ($T=31$ and 180 °C), thermal vacancies cannot trap positrons,[14] indicating that nonthermal trapping occurs for positrons with energy $-\phi_+<E<0$.

d. Indium. In contrast to previous metals, In shows pronounced thermal-vacancy trapping below the melting point. The positron work function[52] in In is $\phi_+=2.6\,\mathrm{eV}$; thus, only positrons with $E>\phi_+$ are reemitted. The fraction of incident positrons that are reemitted at $E=70\,\mathrm{eV}$ from the surface of In was $\approx$11.4%. As with Bi, Sn, and Na, this fraction is small (compared with Al) because of the large positron work function, and the diffusion length is not greatly affected by

TABLE II. Change in the bulk value of the S parameter below and above the melting point. The largest change is observed in metals where positrons do not get trapped in thermally generated vacancies in the solid phase. Changes in Ps fraction f_o across the melting point also are shown. The error is quoted in parentheses and corresponds to the last significant digit.

Metal	S_{bulk} below T_m	S_{bulk} above T_m	F_0 below T_m	F_0 above T_m
Ga	0.474(1)	0.488(1)	0.36(2)	0.36(2)
Bi	0.436(1)	0.439(1)	0.90(2)	0.91(2)
Na	0.539(1)	0.545(1)	0.28(4)	0.23(4)
Sn	0.447(1)	0.458(1)	0.79(1)	0.79(1)
Pb	0.430(1)	0.43(1)	0.96(1)	0.94(1)
In	0.446(1)	0.446(1)	0.91(1)	0.87(1)

nonthermal positrons. The sample was measured at 31 and 152 °C (solid In) and at 165 °C (liquid In).

V. CONCLUSIONS

Using a vertical positron beam, we measured the Doppler broadening of annihilation γ rays from positrons in six liquid and solid metals. Preliminary results from Ga and Bi presented by Gramsch *et al.*[16] indicated large differences between the solid and liquid phases of metals. From Doppler broadening measurements, we calculated the diffusion coefficient of positrons in liquid metals and the binding energy of positrons and positronium to solid and liquid metallic surfaces. The aim of this work was to extract information on density fluctuations of the ions in a liquid by measuring the diffusion coefficient of positrons. We found that the diffusion length strongly depends on the density fluctuations, and the diffusion of positrons, at least in liquid Ga, is a hopping process between traps. For other metals, it is still related to density fluctuations, but it may not be related to hopping.[23] This very interesting mechanism differs from the mechanism responsible for diffusion in solids, i.e., scattering with phonons.

We also were interested in the changes of the surface potential caused by melting. Measurements of positronium formation, as well as of the fraction of nonthermal positrons released from the surface, allowed us to determine the change in the surface potential and the branching ratio of positrons or positronium.

The metals studied were Ga, Bi, Na, Sn, Pb, and In. The primary reason for using them was their low melting point and low vapor pressure in the liquid phase which allows to measure Doppler broadening at ultrahigh vacuum ($\sim 1\times 10^{-9}$ torr) with a clean surface.

The S parameter was measured as function of the temperature for all samples. Table II summarizes the bulk S parameter across the melting point. These results show that the bulk S parameter (S_M) is sensitive to whether positrons are freely diffusing or in a trapped state and are consistent with previous Doppler broadening[9–11,15,55] and lifetime experiments.[12,13,44,56] An appreciable change is observed in S_M at the melting point. Metals that do not trap positrons in the solid phase (Ga, Bi, Na, Sn) show a large increase in S_M upon melting; we interpret this effect as due to the creation of centers that can trap positrons in the liquid phase. Most likely, these centers are regions where the ion density is lower than the average.

TABLE III. Results from the fit to the thermal desorption of Ps using Eq. (10). E_a is the formation potential for Ps, E_b is the binding energy of positrons to the surface potential, and F_e is the fraction of nonthermal positrons reaching the surface that are emitted as Ps directly, after being implanted at $E\sim 0$. f_{ts} is the fraction trapped at the surface, Γ is the desorption rate of positrons from the surface at high temperatures, and λ is the annihilation rate at the surface state. The error is quoted in parentheses.

Metal	E_a (eV)	F_e	f_{ts}	Γ/λ (10^4)	E_b[a] (eV)	E_b[b] (eV)	Surface states
Ga	0.35(3)	0.36(1)	0.55(1)	1.0(4)	3.19	2.3	yes
Bi	0.31(3)	0.38(1)	0.59(2)	0.5(1)	2.72		yes
Na						2.7	no
Sn	0.23(1)	0.467(4)	0.47(1)	0.05(1)	2.63	2.5	yes
Pb						2.8	yes
In	0.25(1)	0.47(3)	0.46(2)	0.8(2)	3.25	2.4	yes

[a]This work.

[b]Theoretical work from Nieminen and Hodges (Ref. 52).

From measurements of the S parameter at the surface, S_s, we deduced that there is no change or only a small one across the melting point (within experimental error), suggesting that the branching ratio for Ps formation or annihilation at the surface is not altered by a change from a crystalline to a disordered structure on melting. Furthermore, the characteristics of the surface state appear to be unchanged upon melting.

By fitting the temperature dependence of Ps formation, we obtained the formation energy of Ps and the binding energy of positrons to the surface. Both results are given in Table III, along with the theoretical calculations of binding energy by Nieminen and Hodges.[52] The experimental results are within 40% of the theoretical results. In contrast to some of their calculations, a stable surface state ($E_b > \phi_+$) was found for all metals except Na.

The fraction of nonthermal positrons reemitted from these metals was not affected by the transition from the solid to liquid phase. The reemitted fraction in Bi (for a beam energy of $E_i = 270$ eV), Na ($E_i = 70$ eV), Sn ($E_i = 70$ eV), and In ($E_i = 120$ eV) remained constant over a wide range of temperature. The positron work function in all metals investigated is very large (2–5 eV), which prevents low-energy epithermal positrons from leaving the sample. These positrons are more likely to be affected by a change in the number of traps[25] due to melting or to an increase in temperature. Thus the fraction that can escape is not very sensitive to melting or to changes in temperature.

Table IV summarizes of the diffusion lengths for the different metals investigated. The largest change in the diffusion length is observed in metals where the state of the positron changes from a Bloch-like state to a trapped state upon melting. In metals that trap positrons in thermally generated vacancies, the drop in the diffusion length upon melting is small or nonexistent. In all liquid metals, the positron seems to be in a trapped state. Diffusion appears to be related to trapping in fluctuations in the ionic structure. The positron

TABLE IV. Diffusion length L_+ results below and above the melting point. The error is quoted in parentheses. The largest change is observed in metals where positrons do not get trapped in thermally generated vacancies. m_+ is the effective positron mass in the low-m^+ state; L_0 is the constant defined in Eq. (12).

Metal	L_+ (Å) below T_m	L_+ (Å) above T_m	m_+[a] above T_m	L_0 (Å/$T^{1/4}$)
Ga	1200(100)	60(5)		
Bi	500(40)	190(20)	$0.8m_p$	40.0(4)
Na				
Sn	750(50)	260(20)	$0.2m_p$	66.1(7)
Pb	180(20)	180(20)	$0.7m_p$	36.8(3)
In	245(20)	225(20)	$0.6m_p$	49.5(3)

[a]m_p is the mass of the proton.

hops from fluctuation to fluctuation. The potential well of the traps strongly depends on temperature, so that when it is increased, the potential decreases and, therefore, the hopping motion increases.

In the liquid phase of all metals, diffusion length increased with temperature. In Ga, the increase is very fast, resembling a thermally activated process; all other metals showed a slow almost linear increase.

Using Seeger's model,[23] the increase of the diffusion length in the liquid phase was fitted using Eq. (12). Plots of the diffusion length and the fitted results are shown in Fig. 24, and the values obtained are presented in Table IV. In all metals studied (except Ga), the positron seems to be in the low-m^+ state, with the effective positron mass being close to the proton mass. The effective mass is shown in Table IV.

The diffusion mechanism of positrons in liquids may be a combination of many diffusion modes: (1) a thermally activated process that depends on the strength of the binding to the trap, and also upon the availability of a void where the positron can jump, and (2) another mechanism that may result from fluctuations in the size (and binding energy) of the traps. In each metal, the relative importance of these mechanisms differs at different temperatures.

VI. FUTURE STUDIES

There are indications that melting of small metal clusters embedded in a larger metal host occurs at temperatures below the melting point. The diffusion length and *S* parameter in the bulk of a metal offer a unique opportunity to study melting of clusters or multilayers. The *S* parameter length in Bi, Ga, Sn, and Na is remarkably different in the solid and liquid phase, offering an opportunity to study the temperature dependence of the melting point of clusters of different sizes. Thus, if a cluster of any of these metals is embedded in another material with different bulk melting point, the change in *S* parameter can reveal any deviation of the melting temperature of the cluster from the bulk melting temperature.

Diffusion length offers the possibility of studying melting of overlayers of different metals. For example, a multilayer of Al/Sn/Al should show an increase in the *S* parameter if the Sn layer melts, and simultaneously, there should be a large decrease in the diffusion length of the Sn layer. If melting in thin layers occurs at temperatures below the melting point or if a large number of defects are created, the *S* parameter or the diffusion length should show a change different from that in the bulk.

An interesting set of experiments is the study of surface melting. Recent studies[73] show that the open-packed surfaces of Pb and Al lose their crystalline order a few hundred degrees below the bulk melting point. A roughening transition is seen, even at lower temperatures. The thickness of the molten layer is only a few nm and increases logarithmically as the temperature approaches the melting point.[73] A useful probe of this liquid layer is Ps formation. For several of the metals studied (Bi, Na, Pb, and In), a decrease in the Ps fraction was observed upon melting. Because Ps is very sensitive to surface conditions, it may be an ideal probe for surface melting. A gradual decrease in the Ps fraction might be observed in open-packed surfaces like Pb(110) approaching the melting point because of the appearance of a liquid layer. In close-packed surfaces that do not show surface melting effects, like Pb(111), only a sudden decrease in Ps fraction should be observed on melting.

ACKNOWLEDGMENTS

One of the authors (I.K.) would like to thank Brookhaven National Laboratory for the hospitality. This work was supported by the U.S. Department of Energy, Division of Materials Science, under Contract No. DE-AC02-76CH00016. One of the authors (E.G.) would like to thank support from Dicyt, Contract No. 05-95-31-GL, and Fondecyt, Contract No. 1961236.

*Present address: Physics Department, Universidad de Santiago, Santiago, Chile; electronic address: egramsch@lauca.usach.cl

†Present address: Materials Research Center, Washington State University, Pullman, WA 99164-2711.

‡Present address: Physics Department, Tokyo Gakugei University, Nukuikitamachi, Koganei, Tokyo 184, Japan.

[1] M. Shimoji, *Liquid Metals* (Academic, New York, 1977).

[2] Y. Waseda, *The Structure of Non Crystalline Materials* (McGraw-Hill, New York, 1980).

[3] N. H. March, *Liquid Metals, Concept and Theory*, Cambridge Monographs on Mathematical Physics (Cambridge University Press, Cambridge, England, 1990).

[4] C. H. Hodges, Phys. Rev. Lett. **25**, 284 (1970).

[5] C. D. Anderson, Science **76**, 238 (1932); Phys. Rev. **41**, 405 (1932).

[6] P. J. Schultz and K. G. Lynn, Rev. Mod. Phys. **60**, 701 (1988), and references therein.

[7] I. K. MacKenzie, T. L. Khoo, A. B. McDonald, and B. T. A. McKee, Phys. Rev. Lett. **19**, 946 (1967).

[8] O. E. Mogensen and G. Trumpy, Phys. Rev. **188**, 639 (1969).

[9] R. N. West, R. E. Borland, J. R. A. Cooper, and N. E. Cusak, Proc. R. Soc. London, Ser. A **92**, 195 (1967).

[10] D. R. Gustafson and A. R. MacKintosh, Phys. Lett. **5**, 234 (1964).

[11] D. R. Gustafson, A. R. MacKintosh, and D. J. Zaffarano, Phys. Rev. **130**, 1455 (1963).

[12] W. Brandt and H. F. Waung, Phys. Lett. **27A**, 700 (1968).

[13] V. H. C. Crisp, D. G. Lock, and R. N. West, J. Phys. F **4**, 830 (1974).
[14] J. H. Kusmiss and A. T. Stewart, Adv. Phys. **16**, 471 (1967).
[15] W. Triftshäuser, Phys. Rev. B **12**, 4634 (1975).
[16] E. Gramsch, K. G. Lynn, J. Throwe, and I. Kanazawa, Phys. Rev. Lett. **67**, 1282 (1991).
[17] B. Bergersen, E. Pajanne, P. Kubica, M. J. Stott, and C. H. Hodges, Solid State Commun. **15**, 1377 (1974).
[18] J. Oliva, Phys. Rev. B **21**, 4909 (1980).
[19] E. J. Woll and J. P. Carbotte, Phys. Rev. **164**, 985 (1967).
[20] E. M. Gullikson and A. P. Mills, Jr., Phys. Rev. Lett. **57**, 376 (1986).
[21] S. Valkealahty and R. M. Nieminen, Appl. Phys. A: Solids Surf. **35**, 51 (1984).
[22] I. Kanazawa, J. Radioanal. Nucl. Chem. **210**(2), 451 (1996).
[23] A. Seeger, Appl. Surf. Sci. **85**, 8 (1995).
[24] A. F. Makhov, Sov. Phys. Solid State **2**, 1934 (1960).
[25] B. Nielsen, K. G. Lynn, and Y. C. Chen, Phys. Rev. Lett. **57**, 1789 (1986).
[26] A. Vehanen, K. Saarinen, P. Hautojärvi, and H. Huomo, Phys. Rev. B **35**, 4606 (1987).
[27] K. G. Lynn and H. Lutz, Phys. Rev. B **22**, 4143 (1980).
[28] K. Ritley and K. G. Lynn, in *Positron Beams for Solids and Surfaces*, edited by P. J. Schultz, G. R. Massoumi, and P. Simpson, AIP Conf. Proc. No. **218** (AIP, New York, 1990), p. 3.
[29] S. C. Sharma, S. Berko, and W. K. Warburton, Phys. Lett. **58A**, 405 (1976).
[30] J. A. Jackman, G. M. Hood, and P. J. Schultz, J. Phys. F **17**, 1817 (1987).
[31] H. Huomo, A. Vehanen, M. D. Bentzon, and P. Hautojarvi, Phys. Rev. B **35**, 8252 (1987).
[32] T. McMullen and M. J. Stott, Phys. Rev. B **34**, 8985 (1986).
[33] E. Gramsch and K. G. Lynn, Phys. Rev. B **40**, 2537 (1989).
[34] R. M. Nieminen and J. Oliva, Phys. Rev. B **22**, 2226 (1980).
[35] A. P. Mills, Jr., Phys. Rev. Lett. **41**, 1828 (1978).
[36] K. G. Lynn and D. O. Welch, Phys. Rev. B **22**, 99 (1980).
[37] R. M. Nieminen and C. H. Hodges, J. Phys. F **6**, 573 (1976).
[38] C. H. Hodges and M. J. Stott, Phys. Rev. B **7**, 73 (1973).
[39] I. K. MacKenzie, J. A. Eady, and R. R. Gingerich, Phys. Lett. **33A**, 279 (1970).
[40] H. Houmo, E. Soininen, and A. Vehanen, Appl. Phys. A: Solids Surf. **49**, 647 (1989).
[41] A. van Veen, H. Schut, J. de Vries, R. A. Hakvoort, and M. R. Ijpma, in *Positron Beams for Solids and Surfaces*, edited by P. J. Schultz, G. R. Massoumi, and P. Simpson, AIP Conf. Proc. No. **218** (AIP, New York, 1990), p. 83.
[42] J. Throwe, K. G. Lynn, E. Gramsch, and I. Kanazawa, in *Proceedings of the International Symposium on Positron Annihilation Studies of Fluids*, Arlington, Texas, 1987, edited by S. C. Sharma (Academic, Arlington, 1988), p. 548.
[43] H. Weisberg and S. Berko, Phys. Rev. **154**, 249 (1967).
[44] D. Segers, C. Dauwe, M. Dorikens, and L. Dorikens-Vanpraet, Appl. Phys. **10**, 121 (1976).
[45] D. T. Britton and P. C. Rice-Evans, Phys. Lett. A **126**, 444 (1988).
[46] G. Petzow, *Metallographic Etching* (American Society for Metals, Metals Park, OH, 1978).
[47] J. Hafner and W. Jank, Phys. Rev. B **42**, 11 530 (1990).
[48] A. P. Mills, Jr., Solid State Commun. **31**, 623 (1979).
[49] I. J. Rosenberg, A. H. Weiss, and K. F. Canter, J. Vac. Sci. Technol. **17**, 253 (1980).
[50] S. A. Chu, A. P. Mills, Jr., and C. A. Murray, Phys. Rev. B **23**, 2060 (1981).
[51] N. W. Ashcroft and N. D. Mermin, *Solid State Physics* (Holt, Rinehart, and Winston, New York, 1976).
[52] R. M. Nieminen and C. H. Hodges, Phys. Rev. B **18**, 2568 (1978).
[53] O. V. Boev, M. J. Puska, and R. M. Nieminen, Phys. Rev. B **36**, 7786 (1987).
[54] A. Seeger, J. Phys. F **3**, 248 (1973).
[55] Y. Kishimoto and S. Tanigawa (unpublished).
[56] D. Segers, M. Dorikens, and L. Dorikens-Vanpraet, Phys. Status Solidi A **48**, 133 (1978).
[57] R. M. Nieminen, in *Positrons in Solids*, edited by P. Hautojärvi (Springer-Verlag, New York, 1979), p. 178.
[58] R. N. West, R. E. Borland, J. R. A. Cooper, and N. E. Cusack, Proc. Phys. Soc. London **92**, 195 (1967).
[59] I. K. MacKenzie, G. F. O. Langstroh, B. T. A. McKee, and C. G. White, Can. J. Phys. **42**, 1837 (1967).
[60] S. Dedoussis, S. Charalambous, and M. Chardalas, Phys. Lett. **62A**, 359 (1977).
[61] Y. C. Jean, K. G. Lynn, and M. Carroll, Phys. Rev. B **21**, 4935 (1980).
[62] B. T. A. McKee, W. Trifthäuser, and A. T. Stewart, Phys. Rev. Lett. **28**, 358 (1972).
[63] S. C. Sharma, S. Berko, and W. K. Warburton, Phys. Lett. **58A**, 405 (1976).
[64] R. H. Howell, I. J. Rosenberg, P. Meyer, and M. J. Fluss, Phys. Rev. B **35**, 4555 (1987).
[65] M. S. Wertheim, Phys. Rev. Lett. **10**, 321 (1963).
[66] C. H. Hodges and H. Trinkaus, Solid State Commun. **18**, 857 (1976).
[67] C. H. Leung, T. McMullen, and M. J. Stott, J. Phys. F **6**, 1063 (1976).
[68] A. P. Mills, Jr., Phys. Rev. Lett. **41**, 1828 (1978).
[69] C. J. Powell, J. Vac. Sci. Technol. A **3**, 1338 (1985).
[70] B. Nielsen, K. G. Lynn, and Y. C. Chen, Phys. Rev. Lett. **57**, 1789 (1986).
[71] A. P. Mills, in *Positron Solid State Physics*, edited by W. Brandt and A. Dupasquier (North-Holland, Amsterdam, 1983), p. 432.
[72] C. Herring and M. H. Nichols, Rev. Mod. Phys. **21**, 185 (1949).
[73] J. W. M. Frenken, P. M. J. Maree, and F. van der Veen, Phys. Rev. B **34**, 7506 (1986).
[74] W. Jank and J. Hafner, Phys. Rev. B **41**, 1497 (1990).
[75] E. Gramsch, Ph.D. dissertation, City University of New York, New York, 1992.